$1.40

HIGHWAY RESEARCH RECORD

Number 107

Nuclear Applications

5 Reports

Presented at the
44th ANNUAL MEETING
January 11-15, 1965

SUBJECT CLASSIFICATION

31 Bituminous Materials and Mixes
33 Construction
34 General Materials
35 Mineral Aggregates
62 Foundations (Soils)

HIGHWAY RESEARCH BOARD
of the
Division of Engineering and Industrial Research
National Academy of Sciences—National Research Council
Washington, D. C.
1966

Special Committee on Nuclear Principles and Applications

(As of December 31, 1964)

Donald R. Lamb, Chairman
University of Wyoming, Laramie

Wayne R. Brown, Colorado Department of Highways, Denver
Louis J. Circeo, Jr., Plowshare Division, Lawrence Radiation Laboratory, Livermore, California
Donald O. Covault, Professor of Civil Engineering, Georgia Institute of Technology, Atlanta
John C. Dempsey, Division of Isotope Development, Atomic Energy Commission, Washington, D. C.
C. Page Fisher, Department of Civil Engineering, North Carolina State College, Raleigh
Robin P. Gardner, Research Triangle Institute, Durham, North Carolina
William H. Goetz, Joint Highway Research Project, Purdue University, Lafayette, Indiana
Hamilton Gray, Chairman, Department of Civil Engineering, Ohio State University, Columbus
George L. Hinueber, Association of American Railroads, Chicago, Illinois
C. S. Hughes, III, Virginia Council of Highway Investigation and Research, University of Virginia, Charlottesville
H. W. Humphres, Assistant Construction Engineer, Washington Department of Highways, Olympia
Harry D. Richardson, Director, Nuclear Science Center, Louisiana State University, Baton Rouge
Arnold E. Schwartz, Department of Civil Engineering, Clemson College, Clemson, South Carolina
Preston C. Smith, Principal Research Engineer (Soils), Materials Division, U. S. Bureau of Public Roads, Washington, D. C.
Peter C. Todor, Florida State Road Department, Gainesville

Foreword

This Record offers five papers that bring together the latest results of research in the area of nuclear principles and applications. These papers cover a wide spectrum from basic principles of nuclear interactions to the use of the fusion-fission aspects for excavation and aggregate production. Even though the concepts discussed here are complex, these papers will be easily read and understood by the layman.

Preiss's paper is concerned with the analysis of the present-day gamma-ray backscatter density gages and this analysis has improved the use of these gages.

As a companion paper, Todor and Gartner evaluate the direct transmission-type density gage as used by the Florida State Road Department.

A great amount of difficulty has been experienced in obtaining the density of mixed-in-place hot asphalt. Brown discusses the development of a test using a nuclear device that provides help in this critical area.

The use of nuclear explosives as an aid to highway engineering is presented in two papers. Hansen and Toman offer a new technique in aggregate production and discuss the present hazards of such an operation. Nordyke and Circeo offer information concerning the latest progress in nuclear excavation technology.

Contents

Analysis and Improved Design of Gamma-Ray Backscattering Density Gages

K. PREISS, Assistant Professor of Civil and Nuclear Engineering, University of Illinois

The nuclear reactions which gamma radiation may undergo in a material of medium atomic weight, such as soil, are discussed and related to the properties of backscattering density gages. Theoretical reasoning and experimental evidence are presented to show that the effect of the chemical composition of the material may be eliminated when: (a) the detector "sees" material near the source, and (b) photons of energy below 0.1 mev are not detected. The latter may be achieved with a scintillation counter and pulse selector or by placing iron filters in front of a Geiger-Müller tube. The geometry defined by (a) causes the peak in the calibration curve to move to a density so high that the count rate becomes a unique measure of density, rising over the entire range of density from 0 to 160 pcf. Errors in the density reading due to the statistics of nuclear counting and surface roughness are discussed.

•INSTRUMENTS which measure the density of soils by gamma-ray backscatter have been in use for some years. There has been conflicting experimental evidence as to whether the type or chemistry of the soil tested affected the instrument reading. Neville and van Zelst (13), Gnaedinger (5), Mintzer (12), Kuhn (9), and others have found such an effect, but Carlton (3) and Huet (8) reported that, for the soils tested, this effect was not observed. The present paper shows that this effect must be expected in instruments for which count rate falls as density increases.

Belcher et al. (1), Carey and Reynolds (2), Kuranz (10), Carlton (3), Lauchaud (11), and Kuhn (9) reported that roughness of the surface beneath the instrument may affect the reading. This cause of error is discussed here.

Much experimental work has been done with gamma-ray backscatter instruments. However, an understanding of the factors which may affect the reading must come from a fundamental knowledge of all the processes which gamma radiation may undergo in the soil. This paper describes these processes and then relates them to the behavior of backscatter density gages.

NOTATIONS

- a = distance from source to detector;
- b = constant equal to R_p/I;
- d = effectively infinite depth;
- h = height of legs on apparatus;
- r = ratio of count on specimen to count on standard;
- p = probability of a photon remaining uncollided;
- t = time interval between calibration and use of instrument;
- x = distance;
- A = atomic weight of element;
- E_0 = energy of photon before collision, mev;

Paper sponsored by Special Committee on Nuclear Principles and Applications.

E_i = energy of photon after collision, mev;
F_i = mass fraction of i^{th} element in material,

$$\sum_{i=1}^{i=n} F_i = 1$$

I = source intensity, photons/sec;
I_c = source intensity at time of calibration;
N = number of pulses detected in T sec;
N_A = Avogadro number, 0.6×10^{24}/mole;
R = net count rate;
R_b = count rate due to background;
R_p = net count rate when density is zero;
R_s = count rate due to scattered photons;
R_T = total count rate;
S = sensitivity $\equiv R'/R$;
T = time interval for detecting N pulses, sec;
Z = atomic number of an element;
Σ = macroscopic reaction cross-section, cm^{-1};
σ = standard error;
ρ = density;
λ = decay constant of source;
ξ = Compton scattering cross-section per electron;
δ = reaction cross-section per atom;
θ = angle of scatter of photon.

PHYSICAL PROCESSES

Sources of Gamma Energy

An element which has been bombarded with elementary particles, so that the atomic nuclei possess excess energy, is unstable. The nuclei will return to a stable condition and in so doing may emit energy. This energy, which appears as particles called photons, is known as gamma energy and the isotope of an element emitting such energy is called a gamma-emitting isotope.

If a source of radiation is placed near a detector for T sec and N photons are counted in this time to give a count rate $R = N/T$, then N has a standard error of $(N)^{1/2}$ due to the fundamental randomness of the radioactive decay process (4):

$$R = N/T \pm (N)^{1/2}/T \qquad (1)$$

This relation is used later.

Nuclear Cross-Sections

If a beam of energy photons penetrates a material, the photons may collide with the particles constituting that material. The probability that any one photon remains uncollided in distance x is

$$p = e^{-\Sigma x} \qquad (2)$$

where Σ, the mean number of collisions per unit length for a beam of unit cross-section, is known as the macroscopic collision cross-section and is a measure of the probability that a collision will occur.

The probability that a particular type of colliding reaction will occur between a photon and any atom (i.e., the cross-section per atom for the reaction) is usually known from fundamental considerations. The cross-section per atom is related to the macroscopic cross-section in the following way: cross-section per cubic centimeter cm = cross-section per atom × number of atoms per cubic centimeter. By Avogadro's law the number of atoms per cubic centimeter of an element is $N_A\rho/A$, where N_A is Avogadro number, ρ is density and A is atomic weight of the element. Therefore,

$$\Sigma = N_A\rho\delta/A \tag{3}$$

where δ is the cross-section per atom.

When a beam of gamma photons enters a mass of soil, many reactions may occur between the photons and the atoms in the soil, but the only reactions of significance in this technique are Compton scattering and photoelectric absorption.

Compton Scattering

Compton scattering is the scatter of a photon by an orbital electron. In this process, the binding energy of the electron to the nucleus has no effect. The cross-section per electron is given by the Klein-Nishina formula (4) and is dependent only on the incident photon energy. If ξ is this cross-section per electron, the cross-section per atom is $Z\xi$ and from Eq. 3 the macroscopic cross-section $\Sigma = N_A\rho Z\xi/A$.

If the material is composed of n elements, the mass fraction of each being F_i, then the mass of each element per cubic centimeter is $F_i\rho$ and the macroscopic cross-section is given by

$$\Sigma = \sum_1^n N_A\rho F_i Z_i \xi/A_i = N_A\rho\xi \sum_1^n F_i Z_i/A_i \tag{4}$$

At each scatter a photon loses energy. If E_0 is the incident energy, and θ is the angle of scatter, the energy of the scattered photon E_1 is given by (4):

$$E_1 = \frac{E_0}{1 + \frac{E_0}{0.511}(1 - \cos\theta)} \tag{5}$$

Photoelectric Absorption

In photoelectric absorption processes, the photon is absorbed by collision with an orbital electron tightly bound to the nucleus. The cross-section per atom is given approximately (14) by $\delta = 1.25 \times 10^{-9}\, Z^5 E_0^{-7/2}$. Therefore, $\Sigma = kN_A\rho Z^5/A$, where $k = 1.25 \times 10^{-9}\, E_0^{-7/2}$. For a material comprising n elements, $\Sigma = kN_A\rho \sum_1^n Z_i^5\, F_i/A_i$.

It should be noted that the quantity Z/A is very nearly ½ for all elements except hydrogen, for which it is almost 1. However, the mass of hydrogen per unit volume in soil is small because hydrogen is very light. Preiss and Newman (17) calculated the quantities $\sum_1^n F_i Z_i^5/A_i$ and $\sum_1^n F_i Z_i/A_i$ for a wide range of materials and showed that the former varies from one material to another but the latter varies hardly at all. Therefore, absorption processes depend strongly on the elemental constitution of the

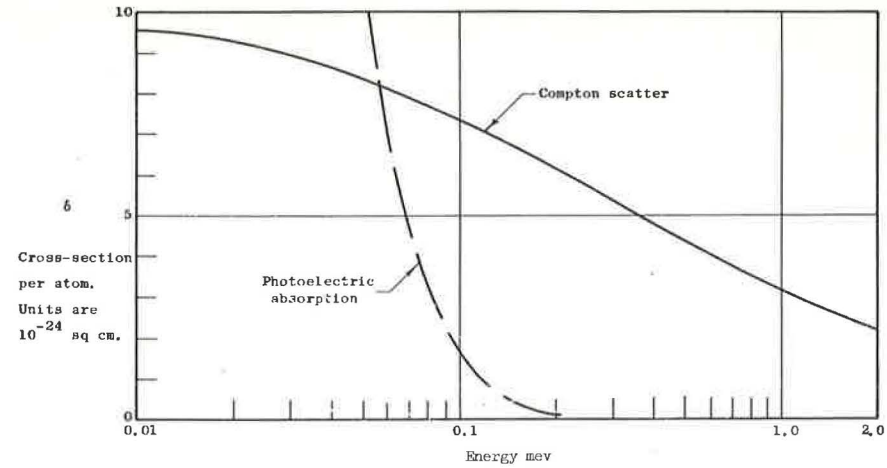

Figure 1. Photoelectric absorption and Compton scattering cross-sections per average atom of soil or concrete (Z = 15, A = 31) as a function of incident photon energy (from Grodstein, 1957).

material and scattering does not. It is apparent that any technique devised to measure the density of soils over a large range of soil types should be based on Compton scattering processes, with the influence of the photoelectric absorption reaction reduced to a minimum or entirely eliminated.

None of these processes depends on interatomic, crystalline or other forces. Although, in general, these forces may influence energy quanta, the effect at this range of energy is negligible. Gamma density methods measure the number of atoms per unit volume without regard to chemical binding forces and effects and, therefore, are insensitive to the structure of the material. For this reason, experimental results obtained on concretes are applicable to soils and vice versa.

Figure 1 shows the cross-sections for photoelectric absorption and Compton scattering as functions of photon energy. It is seen that between 0.1 and 2 mev, Compton scattering is the only effective process. If, therefore, an apparatus can be made so that the photon energies are always in this range, the effect of chemical composition will be very small. It is shown in the following sections that such a solution is achievable when the detector "sees" the soil near the source.

CALIBRATION CURVES AND SOURCE-DETECTOR GEOMETRY

The general shape of the calibration curve for a backscatter density gage is shown in Figure 2. At zero density, no photons are scattered back to the detector, and the count rate R = 0. As the density of the material increases, two opposing processes occur. Although more photons are scattered towards the detector, photons directed towards the detector are again scattered and move away from it. At low densities, the number of scatters experienced by a detected photon is low, perhaps only one scatter. An increase in density in this range causes an increase in the count rate as the number of once- or twice-scattered detected photons increases. On the rising portion of the curve, the photons will have lost little energy.

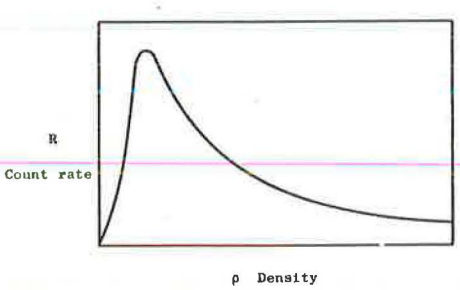

Figure 2. Calibration curve for backscatter density gage.

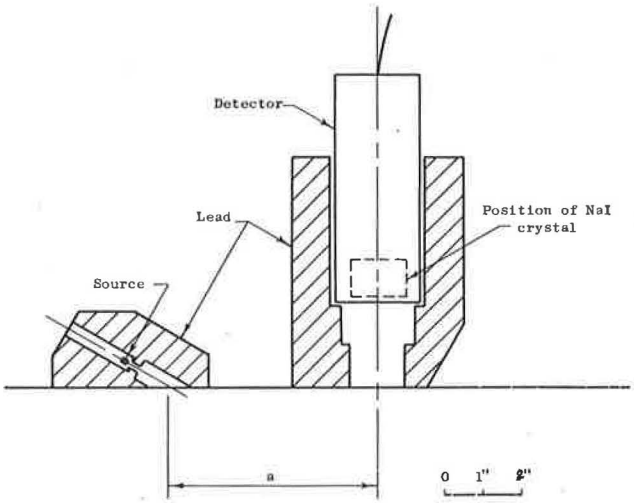

Figure 3. Source and detector arrangement for obtaining results with different geometries.

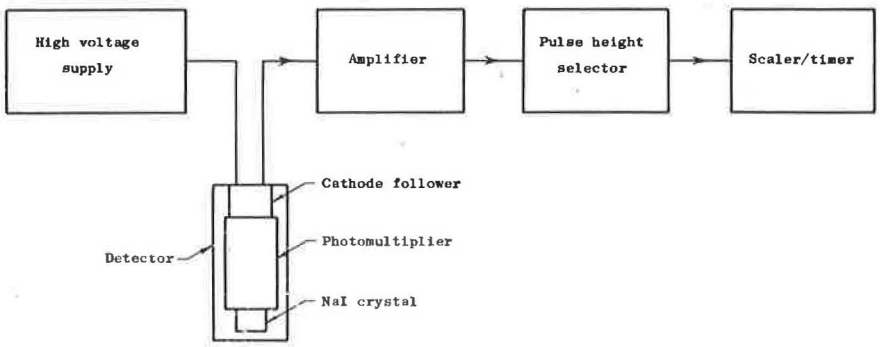

Figure 4. Block diagram of detection system.

At some density, the multi-scatter process begins to predominate; as few once- or twice-scattered photons survive to detection, the curve falls. As density increases further, the photons scatter more until their energy is reduced to that region in which photoelectric absorption probability is high. Thus, as $\rho \rightarrow \infty$, $R \rightarrow 0$.

This hypothesis was tested experimentally using a scintillation counter with the apparatus shown in Figure 3. The source shield, which provided a collimated beam of photons, could be placed at any distance from the detector shield. The latter insured that the detector "saw" radiation only in a restricted volume.

Scintillation counters have the very useful property that the height or voltage of a pulse due to a detected gamma photon is proportional to the energy lost by that photon in the scintillator. By electronic sorting and counting of the pulses, the energies of photons being detected can be determined.

The detector (Fig. 4) consisted of a sodium iodide (NaI) scintillating crystal, $1\frac{1}{2}$ in. in diameter and 1 in. thick, coupled by silicone grease to a photomultiplier. From the photomultiplier, the pulses were passed to a cathode follower, linear amplifier and then a pulse height selector, which passed only these pulses of amplitude (energy) falling within a preselected range. From the pulse height selector, the pulses passed to a scaler-timer unit for determining the count rate. By taking a series of counts over different ranges of pulse height, the pulse height distribution was obtained.

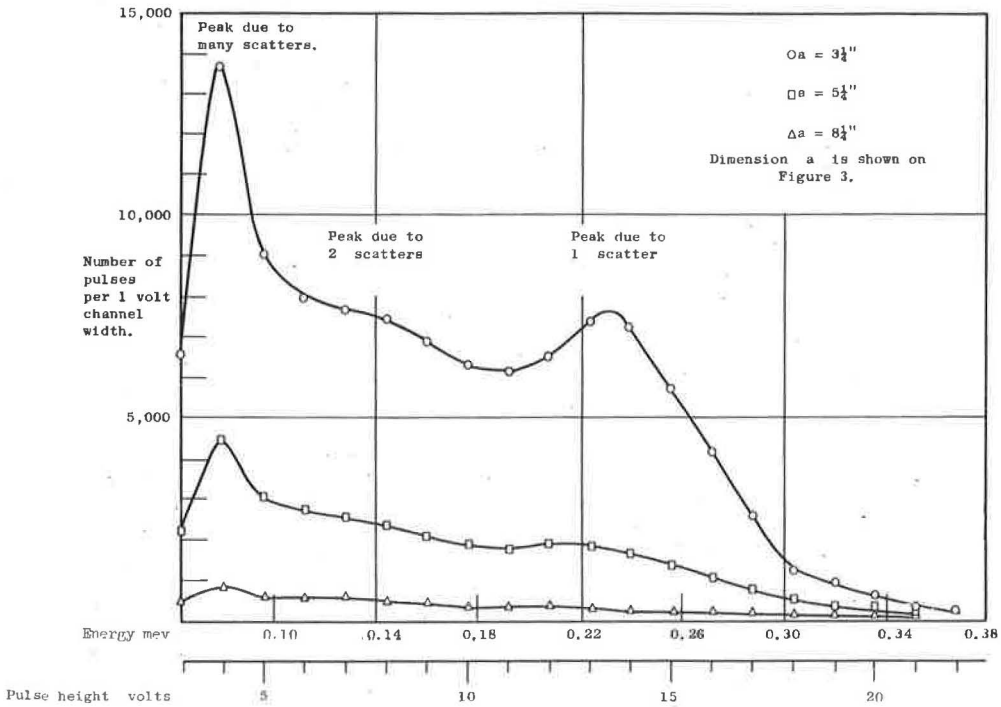

Figure 5. Pulse height distributions obtained on concrete block of density of 156 pcf using Cs-137, with various distances between source and detector.

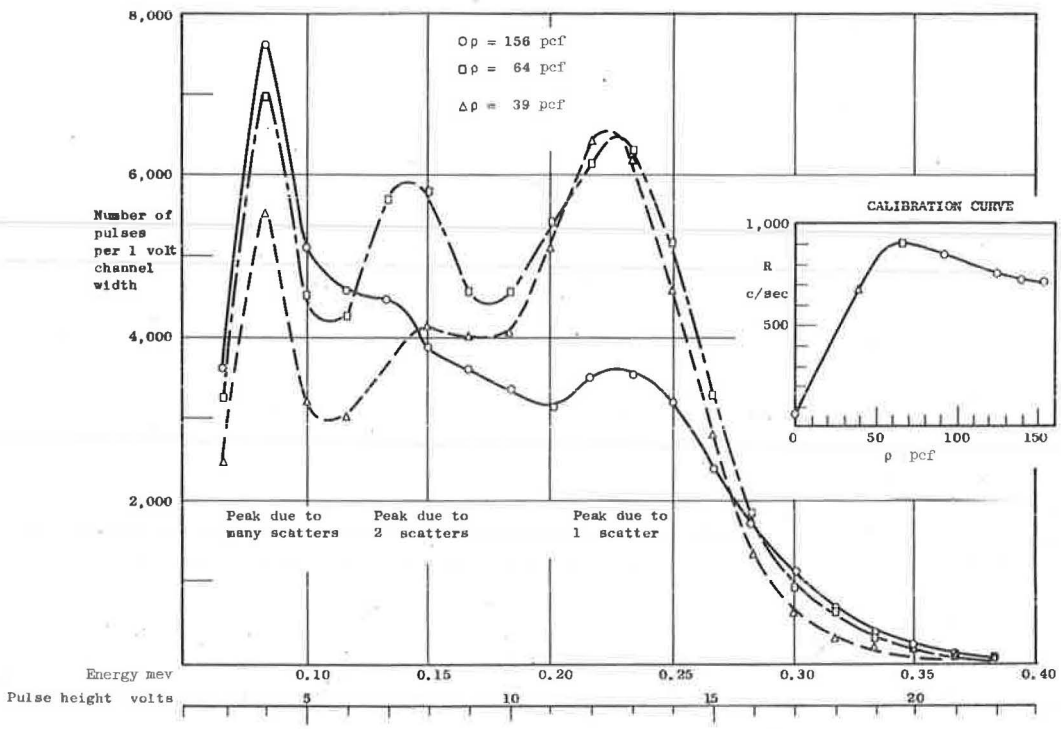

Figure 6. Calibration curve and pulse height distributions for a particular geometry (dimension a = $4\frac{1}{4}$ in.) on blocks of various densities.

Figure 5 shows the pulse height distributions obtained on a concrete block with a density of 156 pcf using a source of cesium 137 (source energy of 0.662 mev) with various distances from source to detector. As the distance from source to detector was increased, the relative intensity of high- to low-energy pulses decreased; i.e., the radiation became more times scattered.

The source energy was 0.662 mev, and the energy after scattering through 120 deg was calculated from Eq. 5 to be 0.224 mev. Therefore, the peak at that energy was due to the once-scattered photons. The peak at about 0.13 mev, small in Figure 5 but much larger in Figure 6, was due to twice-scattered photons. It has been observed (6, 7) that in a system such as this where the photons scatter through a given angle, by one, two or many scatters, the twice-scattered photons give a peak in the spectrum. The energy of twice-scattered photons was calculated as a function of scattering angle; for a Cs-137 source and a total angle of scatter of 120 deg, photons which suffered an initial large-angle scatter had final energy near 0.13 mev, giving the peak at that energy. At energies below 0.13 mev were photons which had scattered many times. If the concrete were a pure Compton scatterer, showing no absorption, the spectrum would reach infinity asymptotically as $E \rightarrow 0$, but because photoelectric absorption eliminated the lowest energy photons a peak was obtained. Hayward and Hubbell (7), Preiss (15) and others have shown that the position of the highest energy peak is dependent on the energy of the source, but the position of the intermediate energy peak is little affected and the position of the lowest peak is not affected.

Figure 6 shows pulse height distributions taken at three densities at a given geometry, together with the calibration curve at that geometry. At a density of 39 pcf, the number of once-scattered photons at 0.224 mev was relatively great and the calibration curve was rising. At 64 pcf, the relative number of twice- and more-times-scattered photons had increased and the calibration curve was at its peak. At 156 pcf, the number of once- and twice-scattered photons was reduced, most of the count rate was due to much scattered photons, and the calibration curve was falling.

If, therefore, the apparatus is arranged so that predominantly once- or twice-scattered photons are detected, the calibration curve will rise with density over the entire practical range. If, in addition, the detector is designed so as not to detect photons of energy less than 0.1 mev, the effect of photoelectric absorption and, therefore, of chemical composition will be minimized.

If the shield geometry is such that the calibration curve is a falling function of energy, the radiation will be much scattered and almost all the photons will be below 0.1 mev. If a bare Geiger-Müller detector is then used, low-energy photons will be detected, the photoelectric absorption reaction will be significant and an effect of the chemical composition of the soil must be expected.

When the detector "sees" soil near the source, high- and low-energy photons will be detected. The detection of photons of energy less than 0.1 mev must be avoided by using either a scintillation counter with appropriate pulse height selector or a Geiger-Müller tube with iron filters. In the latter case, the iron will absorb most of the low-energy photons before they reach the detector, but most of the higher energy photons will penetrate the iron. This method of eliminating the effect of chemical composition on the reading is analogous to the use of a cadmium cover for the same purpose in a neutron-scattering water content gage (16).

DESIGN OF BACKSCATTER GAGE

Based on the preceding principles, a backscatter gage was designed and calibrated.

Source

The source energy should be in the range of 0.1 to 2 mev so that the photons are subject to Compton scattering only. Practical sources in that energy range are cesium 137 and cobalt 60 (1.25 mev). Preiss (15) showed that source energy has little effect on the calibration curve. Cs-137, being easier to shield than Co-60 and having a longer half-life, was chosen; 5 millicuries being used.

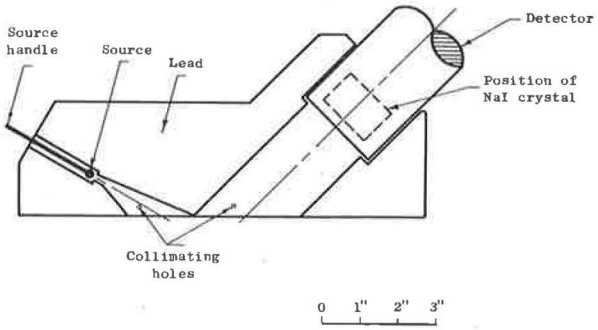

Figure 7. Backscatter gage.

Shield

In order that the detected beam should include a high proportion of once- and twice-scattered photons so that the calibration curve will be a rising function of density and will be due to photons of energy greater than 0.1 mev over all practical ranges, the detector must "see" the material where the photons enter it. However, the detector itself must be separated from the source by several inches of lead to reduce the component of the count rate due to photons penetrating through the lead from source to detector. The geometry of the lead shield (Fig. 7) satisfied these requirements.

Detector

The scintillation counter previously described was used with the pulse height selector set to pass only pulses exceeding 5 volts, which corresponded to 0.1 mev.

CALIBRATION OF GAGE

Sixty concrete blocks, each 12 by 10 by 8 in., were made from a considerable range of concrete mixes. The mixes included mortars comprising ordinary portland cement

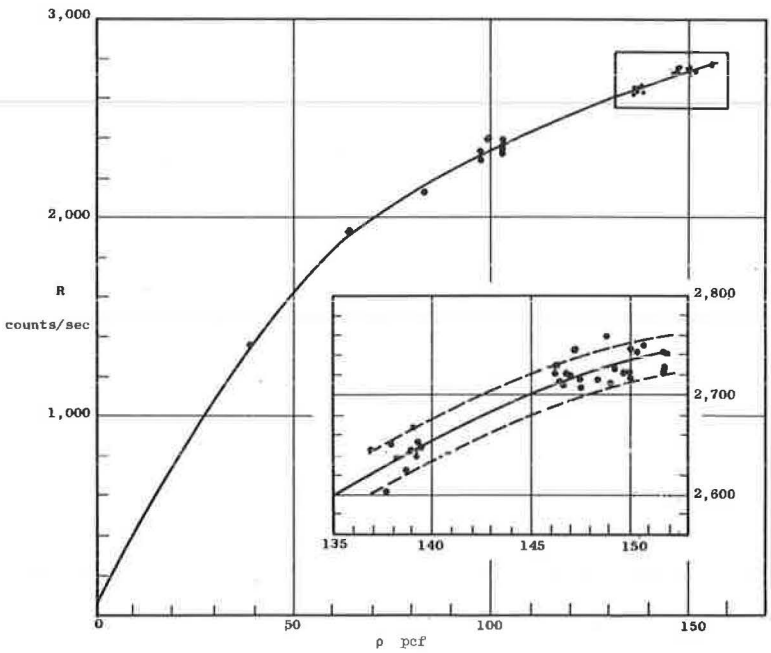

Figure 8. Calibration curve.

and a natural river sand, as well as concretes containing coarse aggregates including granite, river gravel, limestone, and expanded shale lightweight aggregate. The mix proportions were varied, the mixes having water-cement ratios ranging from 0.45 to 0.65 and aggregate-cement ratios ranging from 1.5 to 7.5. At densities below 100 pcf, larger factory-made lightweight blocks were used. Each block tested, therefore, had a chemical composition different from every other. It was shown earlier that the results obtained on the concrete blocks must be valid on soils.

The overall bulk density of each block was measured by weighing in air and water, and a count was taken with the apparatus. A curve of count rate against bulk density by weighing is shown in Figure 8, where the broken lines represent ± 2 standard errors due only to the statistics of nuclear counting; i.e., one point in 20 should, on the average, fall outside the broken lines.

The calibration curve is a curve of local density under the gage against overall density of the block, and this gave rise to apparent errors in the curve. Nevertheless, although the blocks covered a great variety of compositions, the scatter of the points was not much greater than would be expected from the statistical errors due to the randomness of nuclear decay.

ERROR DUE TO STATISTICS OF NUCLEAR COUNTING

The total count comprised radiation scattered off the concrete R_S, radiation penetrating the lead shield R_p, and background radiation due to cosmic and other sources R_b: $RT = R_S + R_p + R_b$. The background count R_b must always be subtracted to give the net count rate

$$R = R_S + R_p \tag{6}$$

For a given instrument, R_S is a function of density and R_p is a constant.

The expression relating density and count rate at a given source intensity I should be $R_S = I\,F(\rho)$. The exact form of $F(\rho)$ is not relevant to this discussion. If $R_p = b\,I$, where b is a constant,

$$R = I\,F(\rho) + b\,I \tag{7}$$

If the count rate R is derived from N counts in T sec and if $R_b \ll R$, the standard deviation of R, from Eq. 1 is $\sigma_R = R/(N)^{1/2}$.

If the second derivation of R with respect to ρ is small, $R(\rho)$ may be assumed to be linear over a small interval and $\sigma_R/\sigma_\rho = dR(\rho)/dp \equiv R'(\rho)$. Therefore,

$$\sigma_\rho = \sigma_R/R' = R/R'\,(N)^{1/2} \tag{8}$$

$$= [F(\rho) + b]/F'(\rho)\,(N)^{1/2} \tag{9}$$

$$= 1/S\,(N)^{1/2} \tag{10}$$

The factor R'/R is defined as the sensitivity of the apparatus, designated S. It is independent of the source intensity and is a function of ρ. To be used as a general measure for gamma backscatter apparatus, the value must be quoted at some standard density. If S is negative at this density, count rate is a falling function of density; if positive, it is a rising function. The accuracy obtainable may be completely specified by quoting both S and R at the standard density.

The factor $(N)^{1/2}$ depends only on the number of counts taken.

The upper limit of S is reached as $R_p \to 0$, and is $F'(\rho)/F(o)$. The time T required to achieve a given standard error is given by

$$T = N/R = 1/S\,I\,F'(\rho)\,\sigma_\rho^{\,2} \tag{11}$$

If the apparatus is calibrated when the source intensity is I, the source intensity any time t thereafter is given by $I = I_c e^{-\lambda t}$. If, therefore, the relation between T and σ_ρ is determined at a given density at any time t = 0, the relation at time t will be $T = e^{\lambda t}/S\, I_c\, F'(\rho)\, \sigma_\rho^2$.

As the source decays, the time required to achieve a given standard error increases. For Cs-137, this increase is about 2 percent per year. Unless the ratio of count on specimen to count on standard is used, the calibration curve must also be changed as time progresses.

If the count rate is changed by ΔR due to surface roughness or another cause, the apparent error in density will be $\Delta\rho = \Delta R/RS$.

The value of sensitivity for the apparatus shown in Figure 7 was 4.0×10^{-3} cu ft/lb at a density of 100 pcf and gave a standard error of 0.3 pcf in 5 min. This error has since been reduced by better design of the apparatus geometry.

If, the ratio of count on the specimen to count on the standard, is used as the ordinate of the calibration curve, the sensitivity S just defined is given by $S = r'/r$, where $r' \equiv dr/d\rho$, and $\sigma_\rho = 1/S\sqrt{1/N_1 + 1/N_2}$.

Thus, using the ratio gives no change in sensitivity, but the calibration count N_1 must be made several times larger than the specimen count N_2 to give an error comparable with that of the count rate against density curve.

REDUCING INFLUENCE OF SURFACE ROUGHNESS ON COUNT RATE

Roughness of a surface may be considered to raise the shield effectively above the "true" surface, reducing the path length between source and detector and, therefore, increasing the count rate. Since the base of the lead shield was plane, 4 in. wide by $10\frac{3}{4}$ in. long, any protuberance over this area would have raised the shield and changed the count rate. Positioning three legs around the source and detector holes in the base is a logical method of reducing this effect (1, 2, 9).

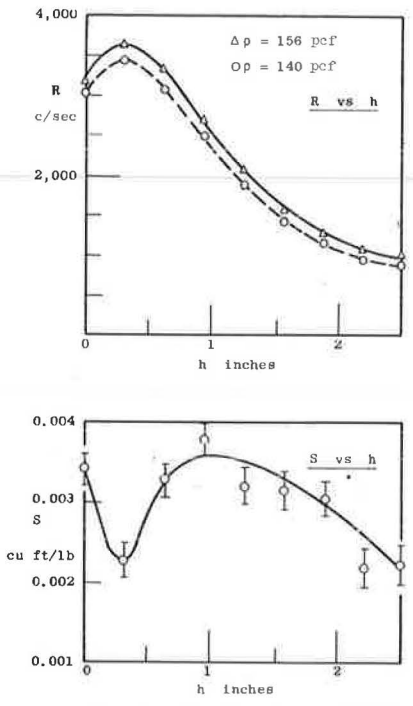

Figure 9. Count rate R and sensitivity S against leg height h.

The roughness of a surface compared with a plane surface may be defined by that height above the plane which gives the same count rate as the rough surface. Therefore, to reduce the effect of roughness, the apparatus should be used on legs of height h corresponding to a low value of the slope of the R vs h curve. This curve can easily be established experimentally.

Readings of count rate against height above a plane surface were taken using the apparatus of Figure 7 on two blocks of concrete, each 16 by 16 by 8 in. and with densities of 156 and 140 pcf. The curve of count rate against height above the surface is shown in Figure 9. Sensitivity at 140 pcf was calculated, assuming a linear calibration curve between 156 and 140 pcf; the curve of sensitivity against height is also shown in Figure 9.

For elimination of the effect of surface roughness on the reading, the legs should be of a height where the slope of the R vs h curve is a minimum. The peak at h = 0.3 in. was probably too sharp to eliminate this effect satisfactorily; therefore, a height of 2.5 in. is more advisable for this shield. The statistical accuracy attainable in a given time at h = 2.5 in. was,

however, reduced by changes in both count rate and sensitivity, so that, for this apparatus, reduction in the influence of surface roughness would have been attained by a sacrifice in time of count or accuracy.

EFFECTIVELY INFINITE DEPTH

It is important to know to what depth the instrument will "see". Hayward and Hubbell (7) showed that the most-scattered photons penetrate furthest into a material, a result which may be expected. The effectively infinite depth is, therefore, determined by the low-energy photons shown in the distributions of Figures 5 and 6.

The probability that a photon survives distance d from the edge of the effectively infinite volume to the concrete surface, derived from Eqs. 2 and 3, is given by

$$p = e^{-N_A \rho \delta d/A} \tag{12}$$

where d is the effectively infinite depth.

For a given material cross-section δ will be a function only of photon energy. The relevant photons are, however, all at the low-energy peak of Figures 5 and 6 so that δ is constant. If the effectively infinite volume is defined by a constant value of probability p, then, because N_A, A and δ are constant, $d \propto 1/\rho$.

With every geometry of apparatus tested by the author, d was found to be 4 in. at a density of 140 pcf and to be inversely proportional to density. The effectively infinite depth was found to be independent of source energy or the distance between source and detector. The depth to which half the detected radiation penetrated did, however, increase from 1 to $2\frac{1}{2}$ in. as the source and detector were moved from a separation distance of $3\frac{1}{4}$ to $7\frac{1}{4}$ in., at a density of 140 pcf.

CONCLUSIONS

The error in density reading may be due to: (a) inaccurate calibration, (b) electronic drift, (c) chemistry of the soil, (d) surface roughness, or (e) statistics of nuclear counting. Although (a) and (b) are important, they were not discussed in this paper.

It has been shown here that the elemental constitution of the soil must affect the count rate when photons of energy less than 0.1 mev are detected. This occurs when the photons are much scattered and, at the same time, results in a calibration curve which falls as density increases. If only photons of energy exceeding 0.1 mev are detected, the soil-type effect becomes negligible. For these higher energy photons to be detected, the detector must "see" soil near the point at which radiation enters it. Once-, twice-, and more times-scattered photons are then detected. This geometry gives a calibration curve which rises with density. To prevent count of the photons of energy below 0.1 mev, a scintillation counter or filtered Geiger-Müller tube must be used.

The error in density reading due to the statistics of nuclear counting is given by equations whose useful application is in finding the best height of legs to reduce the effect of surface roughness. An example of the effect of leg height on the accuracy of a particular instrument is given. As was shown, the use of the slope of the calibration curve by itself as a figure of merit is meaningless; the ratio of slope to ordinate must be considered.

The effectively infinite depth was found to be 4 in. at a density of 140 pcf and was inversely proportional to density. This result was identical for all apparatus geometries and sources used.

Because it had previously been realized that the soil composition could affect the calibration curve, gages had to be calibrated for each soil. This was not a simple procedure. However, by designing the correct geometry of lead shield and by using the correct detector, the soil-type effect can be overcome.

ACKNOWLEDGMENTS

The work reported here was done in the laboratories of the Nuclear Power Group, Department of Mechanical Engineering, Imperial College of Science and Technology, London. The author is grateful to P. J. Grant of the group and to A. L. L. Baker and K. Newman of the Department of Civil Engineering for encouragement and support.

REFERENCES

1. Belcher, D. J., Cuykendall, T. R., and Sack, H. S. U. S. Civil Aero. Admin. Tech. Dev. Report No. 161, 1952.
2. Carey, W. N., Jr., and Reynolds, J. F. Some Refinements in Measurement of Surface Density by Gamma Ray Absorption. Highway Research Board Spec. Rept. 38, pp. 1-23, 1958.
3. Carlton, P. F. ASTM, STP 293, 1960.
4. Evans, R. D. The Atomic Nucleus. New York, McGraw-Hill, 1955.
5. Gnaedinger, J. P. ASTM, STP 293, 1960.
6. Hayward, E., and Hubbell, J. U. S. Nat. Bur. Std., Rept. 2264, 1953.
7. Hayward, E., and Hubbell, J. Jour. Appl. Phys., Vol. 25, No. 4, 1954.
8. Huet, J. Centre de Recherche Routieres, Brussels, Rept. 75/JH/1961, 1961.
9. Kuhn, S. H. Effects of Type of Material on Nuclear Density Measurements. Highway Research Record No. 66, pp. 1-14, 1965.
10. Kuranz, J. L. ASTM, STP 268, 1959.
11. Lauchaud, R. RILEM Bull. 13, 1961.
12. Mintzer, S. ASTM, STP 293, 1960.
13. Neville, O. K., and van Zelst, T. W. ASTM, STP 293, 1960.
14. Price, B. T., Horton, C. C., and Spinney, K. T. Radiation Shielding. Pergamon Press, 1957.
15. Preiss, K. Thesis, Univ. of London, 1964.
16. Preiss, K., and Grant, P. J. Jour. Sci. Instr. (London), Vol. 41, p. 548, Sept. 1964.
17. Preiss, K., and Newman, K. 4th Int. Conf. on Non-Destructive Testing. London, Butterworths, 1963.

Evaluation of Direct Transmission-Type Nuclear Density Gage for Measuring In-Place Densities of Soils

P. C. TODOR and WILLIAM GARTNER, JR.
Respectively, Assistant Research Engineer and Engineer of Research, Florida State Road Department

The direct transmission-type nuclear density gage has proved to be more accurate and faster than conventional methods. The use of the direct transmission principle seems to eliminate the necessity for several calibration curves. Density tests conducted by research personnel are usually made in areas where the contractor is having difficulty obtaining specified density. The nuclear equipment with its inherent speed has provided a means whereby the once time-consuming task of repeated density tests is considerably reduced. The equipment is also useful for setting up compaction equipment schedules and procedure. The amount of coverage required by a given type of compaction equipment to obtain specified density for an entire job can be determined quickly from one test section, provided extensive moisture or material changes are not encountered.

•THE TIME required to conduct conventional in-place density tests and the many possible sources or error (1) have made necessary a more dependable and less time-consuming method of test. Modern advancements in highway construction, especially in the speed of earthmoving equipment, and expanded construction programs, with emphasis on early completion, have increased the need for a faster method of test.

For these reasons, the Florida State Road Department's Division of Research initiated a comprehensive study of the available conventional and nuclear methods for determining in-place density. Results of the preliminary phases of this study have already been published (1, 2); this is a report on the continuation of the program.

The nuclear density equipment currently available commercially employs either of two principles, backscattering or direct transmission.

1. The backscatter gage (Fig. 1a) transmits gamma rays into the soil, and the rays that are reflected or scattered back by the interactions with electrons of the soil mass are counted.
2. With the direct transmission-type gage (Fig. 1b), the source is inserted into the soil and transmits gamma rays in all directions. The majority of the gamma rays counted have traveled in a relatively straight line from source to detector.

This report describes a laboratory and field evaluation of a direct transmission-type nuclear device manufactured by Troxler Electronic Laboratories of Raleigh, N.C. The purpose is the development of method of determining in-place density for routine control testing in base, subbase and embankment materials.

DESCRIPTION OF EQUIPMENT

The nuclear density-moisture measuring system used in this study consists of three units: (a) a surface density gage, (b) a convertible surface-depth moisture gage, and (c) a portable scaler.

Paper sponsored by Special Committee on Nuclear Principles and Applications.

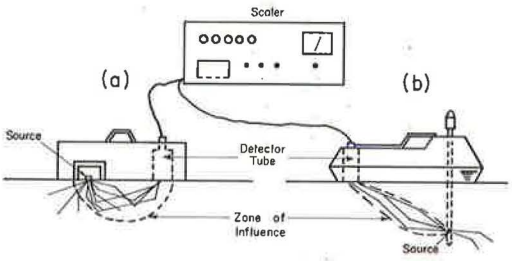

Figure 1. Commercially available nuclear density gages: (a) backscatter, and (b) direct transmission.

Surface Density Gage

The gamma source is radium-beryllium, double-sealed and double-encapsulated in type 304 stainless steel. The standard nominal activity is 3 millicuries, but other activities are available. The detector is a Geiger-Müller detection tube. The source is contained in a steel rod, $\frac{3}{4}$ in. in diameter, which can be lowered into the soil to a predetermined depth of 1 to 9 in. (Fig. 2).

Surface-Depth Moisture Gage

The fast neutron source is also radium-beryllium, double-sealed and double-encapsulated in type 304 stainless steel. The standard nominal activity is also 3 millicuries, but other activities are available. The detector, containing BF, enriched in the B-10 isotope, responds primarily to relatively slow or "thermal" neutrons and shows practically no response to fast neutrons.

The moisture gage was used as a surface gage in this report (Fig. 3); however, it can be used as a depth gage by removing the moisture probe from the surface gage and installing an adapter for the source (Fig. 4).

Scaler Model 200

The scaler, used for both the moisture and density measuring equipment, is transistorized and of modular construction (Fig. 5). Incorporated in the scaler is a mechanical 1-min timer and a rate meter. The selection of operation (moisture or density) is determined by the voltage setting, gain setting and circuit selection. The scaler is battery powered and is furnished with a charger operated from a conventional 115 volt, 60 cycle, a.c. current.

LABORATORY STUDY

The objectives of the laboratory study were (a) to determine whether one or several calibration curves would be required, as was the case in a previous study with a

Figure 2. Troxler surface density gage.

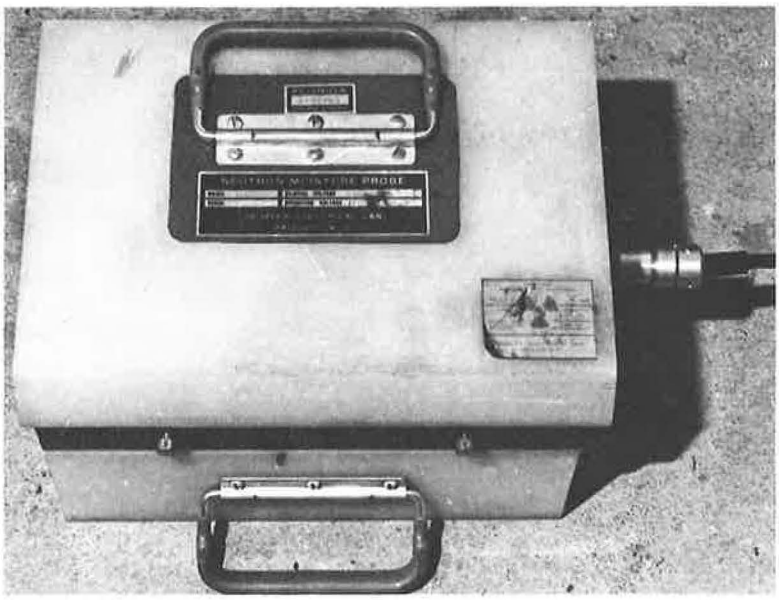

Figure 3. Moisture gage on paraffin standard.

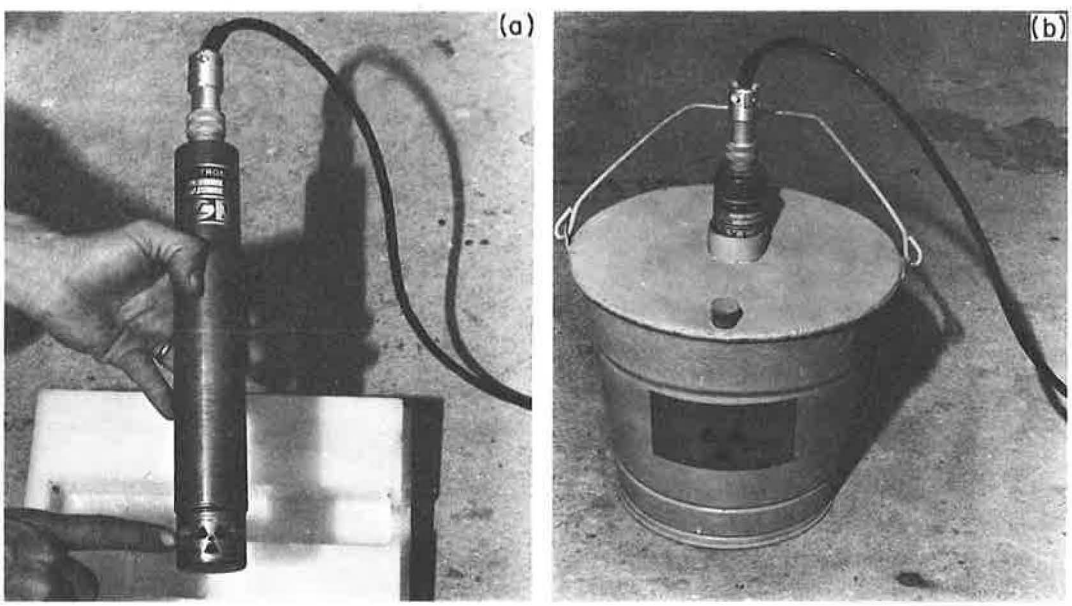

Figure 4. Probe Model 104: (a) removed from surface gage with special attachment, ready for use as a depth moisture probe; and (b) inserted in standard reference.

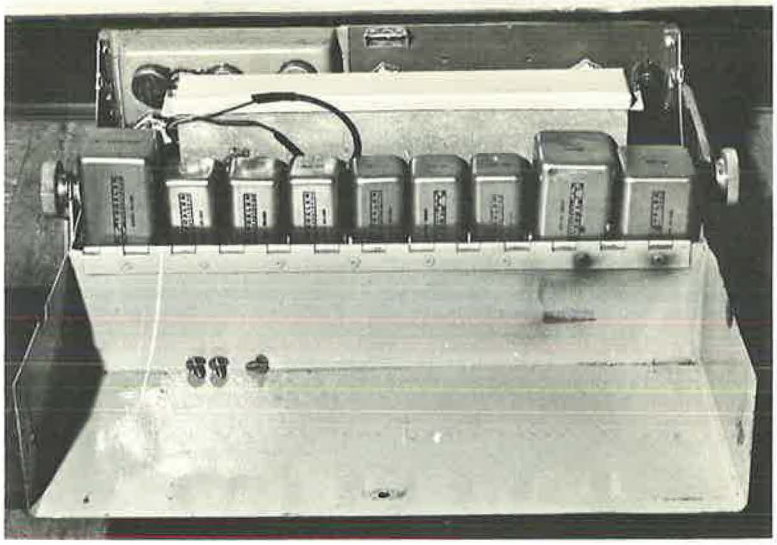

Figure 5. Interior of Model 200 scaler, showing modular type of construction.

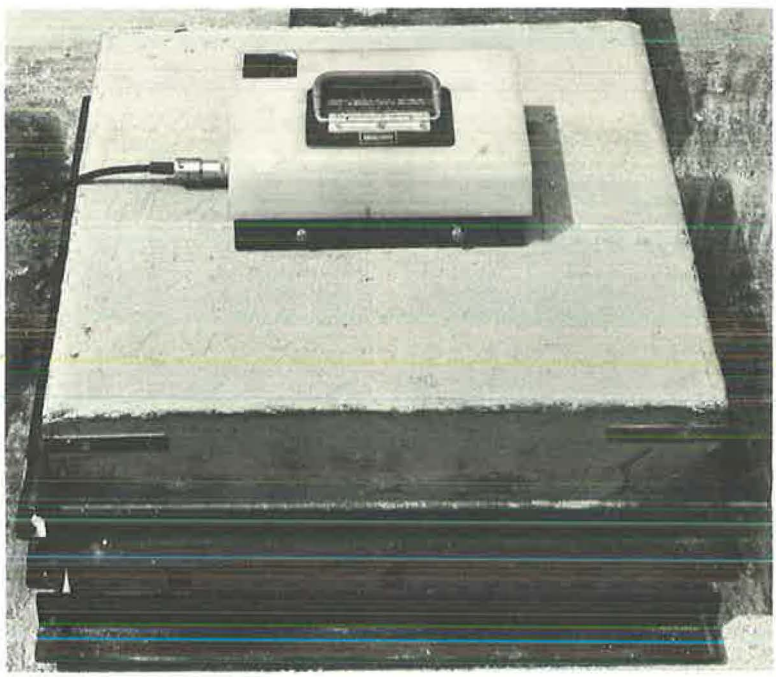

Figure 6. Moisture gage placed in center of sample to obtain moisture count for calibration curve.

backscatter-type device (2); and (b) to establish calibration curves to be used in the field evaluation study. Particular emphasis was placed on determining the extent of radiological safety precautions necessary when using this equipment. This emphasis was continued through the field evaluation.

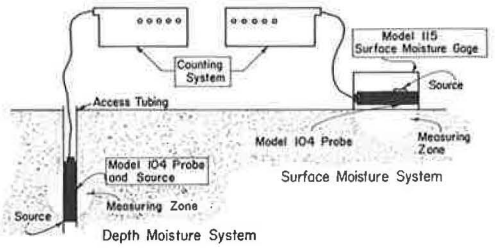

Figure 7. Moisture measuring systems.

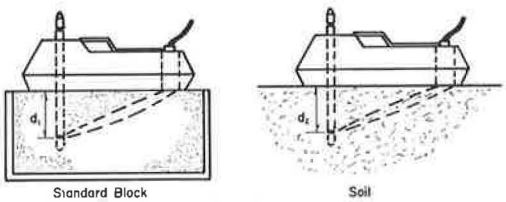

Figure 8. Test procedure using single calibration curve.

Procedure

The laboratory procedure used in this investigation was similar to that used in a previous study (2). Each soil was thoroughly mixed at predetermined moisture contents, covered with a plastic sheet to prevent surface drying, and left standing overnight to allow the moisture to reach a state of equilibrium. The soil was then compacted in boxes of known volume in approximately 2-in. layers to achieve a uniform density, both laterally and vertically, within the box. A collar was constructed which permitted the material to be compacted 2 to 3 in. above the top edge. The collar was then removed and the material was struck off in much the same manner as when preparing a Proctor sample. The entire box was weighed on a platform scale and the average wet density of the material was computed.

The nuclear moisture unit was next standardized (a method whereby the attitude and efficiency of the gage can be numerically evaluated) by taking a series of 60-sec counts on the standard reference paraffin block. The counts were taken until they reproduced themselves within $\pm \sqrt{N}$ (where N = 60-sec count) and then 10 counts were averaged for the standard count. The moisture gage was placed near the center of the sample and a 60-sec count was recorded. Four such counts were recorded with the gage rotated approximately 90 deg between each test (Fig. 6). Samples for ovendry comparison were taken after the density gage counts were recorded.

The nuclear counts resulting from the moisture tests were averaged to obtain a moisture count for the entire specimen. This was divided by the corresponding standard count to obtain the percent of standard. The nuclear moisture gage percent standard was plotted against the oven-dried samples to establish points for the calibration curve drawn as the line of best fit.

Figure 7 is a schematic of the moisture unit being used as a surface gage and as a depth gage. The data reported in this study include only that obtained using the moisture unit as a surface gage. In additional studies, the moisture unit was used as a depth probe and the tests showed favorable agreement with the manufacturer's curve. However, the data available at this time are limited and will not be included in this report.

After completing the moisture counts, the density gage was standardized by taking a series of 60-sec counts on a standard reference concrete block at a 3-in. depth. The counts were taken until they reproduced themselves within $\pm \sqrt{N}$, and then 10 counts were averaged for the standard count. A hole was driven into the material near the center of the box with a hammer and pin. The nuclear density gage was positioned over the hole, the probe was lowered to the desired depth, and three 60-sec counts were recorded. Four such counts were recorded with the gage rotated approximately 90 deg between each test. Tests were conducted at probe settings of 3, 6 and 9 in.

With four locations tested, additional access holes were placed at each corner of the test specimen and tests were conducted with the detector toward the center. Without regard to magnitude, the eight tests were used for an analysis of uniformity. Standard deviations ranged from 0.58 to 2.5 pcf nuclear. Four balloon tests were conducted, one in each quadrant, with deviations ranging from 1.6 to 2.3 pcf.

The materials utilized in the calibration of the nuclear gage included two sources of limerock which varied in calcium content, two sand-clays that varied in iron content, and local sand.

The nuclear counts resulting from tests conducted at each depth were averaged to obtain a density count for the entire specimen. This count was divided by the corresponding standard count to obtain a count ratio for density. The resulting count ratio was plotted against box wet density for each soil tested to establish points for the calibration curve. A regression analysis was made using the method of least squares, assuming a linear relationship to establish a line of best fit for the density curve at each probe depth.

An exercise was conducted to determine the effective depth of test. The sample box was raised above the ground to achieve an air gap beneath the bottom of the box. Density tests were conducted starting at the top at 3-, 6- and 9-in. increments. A 1-in. layer of soil was then removed and the test series was repeated until the probe touched the bottom of the box.

At this point in the program, the field evaluation was initiated. It was soon evident that a calibration curve independent of depth would be very desirable. The equipment was brought back into the laboratory with the intent of establishing such a curve.

A uniform standard was constructed using a single grain-size aggregate, with an access hole that enabled the probe to be inserted to the full test depth of 9 in. in this case. A calibration curve was established, based on the assumption that if the standard count and the soil count were taken at the same depth, the resulting count ratio would be a near constant for all depths since the proportion of mass observed in the standard and in the soil would be the same (Fig. 8).

RESULTS OF LABORATORY STUDY

Utilizing the calibration curve established for the moisture gage, the nuclear moisture gage determinations were compared to the determinations obtained using a conventional Speedy Moisture Kit (3), and both methods were compared with ovendry tests. The results showed that the accuracy of both methods for the several soils tested was within ± 2 percent of the oven-dried samples. Since only one scaler was available, considerable time was saved when the Speedy Kit was used to determine the moisture content and the nuclear gage to determine the wet density.

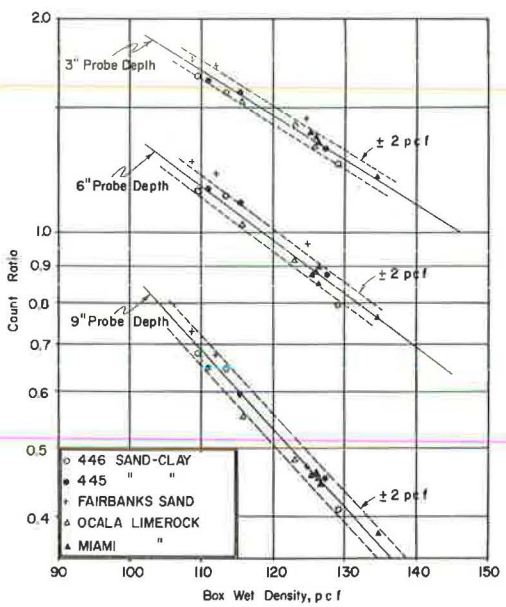

Figure 9. Initial calibration curves for depths of 3, 6 and 9 in.

Because of the sandy soil in Florida, the Speedy Moisture Kit can be used without any difficulty. If the gradation or clay content of a soil would not permit the use of a Speedy Kit, the nuclear moisture gage would be of great advantage since the material would otherwise have to be ovendried.

The initial density calibration curve developed in the laboratory was satisfactory for all of the materials tested (Fig. 9). The accuracy obtained by using a single calibration curve for all materials was well within that obtained in earlier evaluation studies where the backscatter nuclear device was employed with a separate calibration curve for each material (2).

The results of the exercise to determine effective depth are given in Table 1. The tests were conducted beginning at the top and continuing to the bottom without any apparent influence from the air gap beneath the box. The results indicate that the density measured does not include any material below the bottom of the probe. Thus, one has an absolute control over the depth of test.

TABLE 1

RESULTS OF DETERMINATION OF EFFECTIVE DEPTH

Test 1[a]				Test 2[b]				Test 3[c]			
Depth of Probe (in.)	Mat. Removed (in.)	In. Mat. Beneath Probe Tip	Density	Depth of Probe (in.)	Mat. Removed (in.)	In. Mat. Beneath Probe Tip	Density	Depth of Probe (in.)	Mat. Removed (in.)	In. Mat. Beneath Probe Tip	Density
3	0	7	111.5	3	0	7	110.5	3	0	7	105.5
6	0	4	112.0	6	0	4	110.0	6	0	4	105.0
9	0	1	111.0	9	0	1	109.5	9	0	1	106.5
3	1	6	111.8	3	1	6	109.8	3	1	6	105.8
6	1	3	112.5	6	1	3	108.5	6	1	3	106.0
9	1	0	110.8	9	1	0	108.5	9	1	0	105.5
3	2	5	111.0	3	2	5	109.0	3	2	5	104.8
6	2	2	112.8	6	2	2	110.7	6	2	2	106.5
3	3	4	111.5	3	3	4	108.9	3	3	4	105.0
6	3	1	112.0	6	3	1	109.8	6	3	1	106.0
3	4	3	112.5	3	4	3	110.5	3	4	3	105.5
6	4	0	113.0	6	4	0	109.0	6	4	0	104.0
3	5	2	111.0	3	5	2	109.5	3	5	2	106.0
3	6	1	112.5	3	6	1	110.0	3	6	1	105.5
3	7	0	111.8	3	7	0	110.5	3	7	0	105.0

[a]Box density, 111.0 pcf. [b]Box density, 109.0 pcf. [c]Box density, 105.0 pcf.

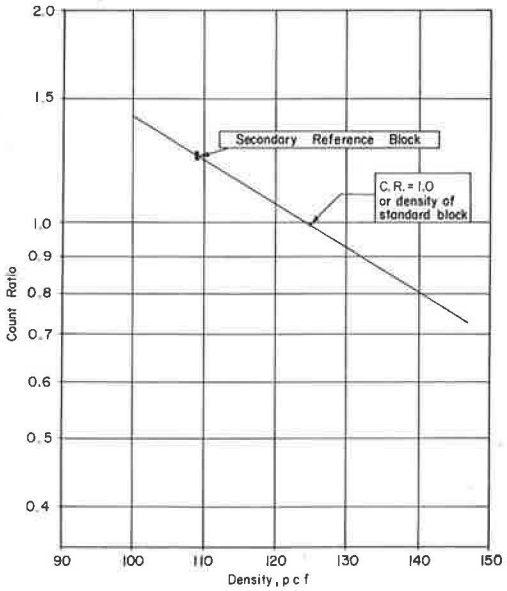

Figure 10. Single calibration curve established using two reference blocks.

Figure 10 shows the single calibration curve for any probe depth between 3 and 9 in. The curve was established by using two standard blocks, plotting the density of the heavier block at a count ratio of 1 and plotting the density of the second block at an average count ratio obtained by counts taken at depths of 1 to 9 in. The results of tests conducted utilizing the single calibration curve are presented in Table 2. The results were consistently within ± 2 pcf of the computed 109.0-pcf density of the secondary reference block, with the exception of the 1- and 2-in. depths.

Difficulty was previously encountered with these depth settings. The density determined at these depths was consistently greater than the computed density. The higher density at these depths may be attributed to the geometry of the source, shielding, and detector. As shown in Figure 11, the lead shielding intercepts a portion of the gamma rays at the 1- and 2-in. probe depths that are otherwise counted at probe settings of 3 in. or more. The reduction in the proportion of gamma rays counted invariably yields a higher density. Since the 1- and 2-in. depths are seldom used in density determinations of soils, the calibration curves for these depths are not presented here. However, future work in the measurement of asphaltic concrete densities will necessitate the establishment of these calibration curves.

Using the single calibration curve, initial tests on compacted samples indicated an apparent need to shift the curve approximately 2 pcf. This was probably caused by inaccuracy in computing the absolute density of the standards and possibly by a portion of the gamma rays escaping the perimeter of the standards. In the soil, these escaped

TABLE 2

DATA USING SINGLE CALIBRATION CURVE ON STANDARD REFERENCE BLOCKS

Depth (in.)	Std. Block	Check Block	Density	Depth (in.)	Std. Block	Check Block	Density
1	25,699	30,450	111.0[a]	1	25,317	29,506	114.0[a]
2	31,262	37,186	111.0[a]	2	29,927	36,411	111.0[a]
3	31,826	39,878	109.0	3	31,009	38,300	110.0
4	29,404	38,068	107.0	4	28,514	35,359	109.0
5	25,640	31,544	110.5	5	25,210	31,612	108.9
6	21,310	26,914	108.9	6	21,184	26,904	110.0
7	17,600	22,405	108.0	7	17,245	22,491	106.5
8	14,570	18,835	107.0	8	14,741	18,978	108.0
9	12,214	15,535	108.0	9	12,213	15,737	108.0
1	44,603	51,272	114.5[a]	1	25,635	30,278	113.0[a]
2	53,018	62,965	112.0[a]	2	30,204	37,396	110.0[a]
3	53,823	67,482	108.9	3	31,726	39,828	109.0
4	50,521	62,979	109.0	4	29,762	37,341	108.5
5	43,674	54,320	109.0	5	26,244	33,148	109.0
6	36,366	46,236	107.5	6	22,078	28,009	109.5
7	30,192	39,038	106.5	7	18,410	23,682	107.5
8	24,670	31,755	108.0	8	15,295	19,499	108.0
9	20,278	26,004	107.0	9	12,456	16,160	107.5

[a]High readings at 1- and 2-in. probe depths result from shielding in gage and indicate that procedures used in this study are not applicable to these shallow depths. A special study is scheduled to establish a separate calibration curve for these probe settings.

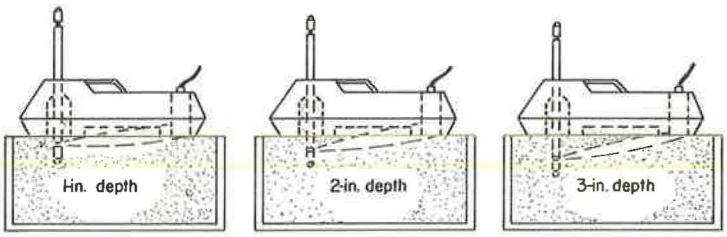

Figure 11. Schematic showing reduction of count due to geometry of source, shielding and detector at the 1- and 2-in. depths.

TABLE 3

RESULTS OF DENSITY TEST ON COMPACTED SAMPLES

Tolerance (pcf)	Prob. of Results Being Within Tol. (%)	
	Nuclear	Balloon
±2	68.2	56.3
±3	86.7	75.8
±4	95.4	88.3
Std. error of Est. (pcf)	1.95	2.33

gamma rays could be reflected back to the detector. A statistical analysis of data obtained with the corrected curve using five different soil types with the tests conducted at 3-, 6- and 9-in. depths is given in Table 3. An error of ±3 pcf would, in Florida materials, be equivalent to a variation of approximately ±2.5 percent in density.

FIELD STUDY

With the laboratory study completed and an equipment calibration curve established which would apparently hold true for

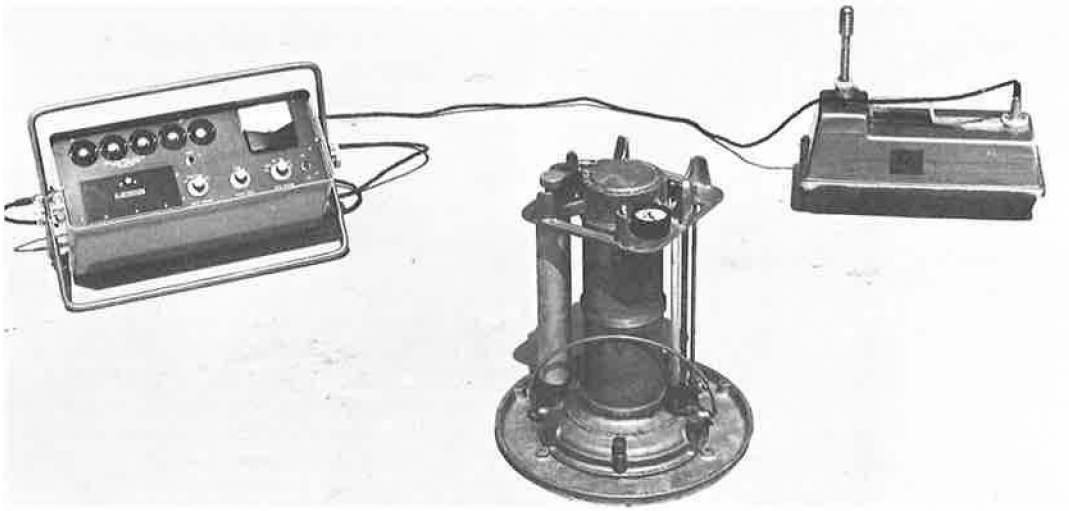

Figure 12. Rainhart Series 200 water balloon, used as comparison of test in field study.

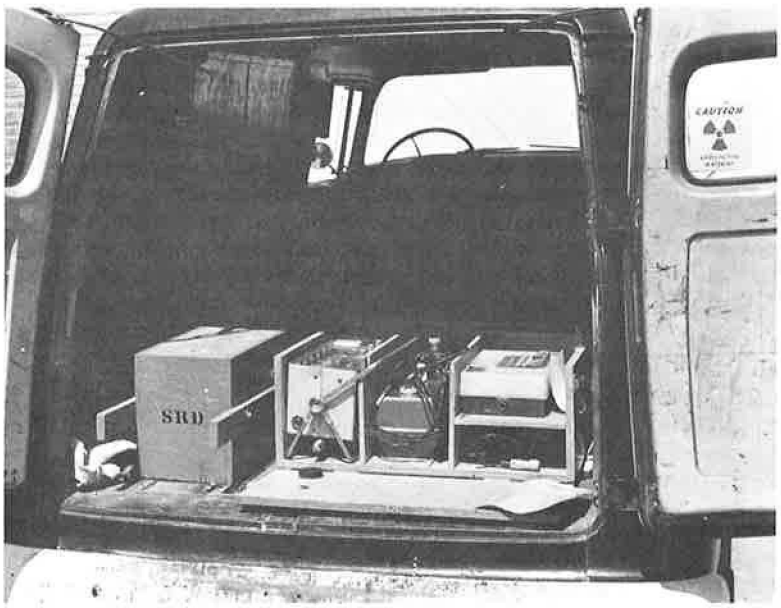

Figure 13. Transportation of equipment for field study.

the wide variation of soil types encountered in the field, the main objectives remaining were to determine the feasibility of using this equipment in the field as a standard control testing device and to determine the ability of the nuclear equipment to function under field conditions. The program also included a study to determine the time required to conduct a conventional destructive-type test and a nuclear test. For this purpose and also to provide a direct comparison of results, a conventional balloon test was conducted at the location of each nuclear test (Fig. 12). The choice of the balloon for the comparison tests was based on previous data obtained (1).

Figure 14. Location of construction sites for field evaluation.

Procedure

Most of the field testing took place on newly constructed subbase and base materials. The equipment was usually transported by a panel truck (Fig. 13). No special care was taken, except to avoid reckless handling of the equipment. The equipment was transported over construction areas throughout the entire state (Fig. 14).

A standard count was taken before each test in the field. The initial field procedure was to standardize the gage before each test. The procedure finally adopted was to standardize the gage before the start of a day's run, and to take a single count on the standard block before each test series. If the single count was within $\pm\sqrt{S.C.}$ (original standard count), it was used. If it was not, another 10-count standard was conducted. It was found necessary to run a standard count in the morning and in the afternoon. A new standard would generally be required for a 20 to 30 deg change in temperature.

After standardization of the equipment, a hole was drilled with a hand auger and the probe was inserted to the desired depth. After satisfactorily seating the gage, three 1-min counts were taken and averaged. The standard count was divided into the average count for the respective count ratio. The calibration curve was then used to determine the wet density.

As mentioned previously, the moisture gage was not used extensively. Instead, the percent of moisture of the material removed with the hand auger was determined by a Speedy Moisture Kit.

At each location, the nuclear tests were conducted first, followed by a Rainhart balloon test conducted between the access hole and the point of the detector at a depth equal to the probe depth.

Time Study

Throughout the field study, a log was kept of the time required to conduct and record a density test by both the nuclear and conventional methods. One phase of the field study included the assigning of a density man equipped with the nuclear gage to several construction projects on which density tests were conducted in limerock base, A-3 and A-2-4 subgrade materials, embankment, pipe backfill, etc. The purpose of this exercise was to determine if one man with nuclear equipment could replace several density crews working on several separate projects.

RESULTS OF FIELD STUDY

Figure 15 represents the relationship determined between the nuclear density gage and the Rainhart water-balloon. For the data shown in Figure 15, 73 percent of the test results agree within ± 2 pcf. There is a little more scattering of results than experienced in the laboratory when both methods were compared to box density; however, an analysis of variance indicated that the amount of scatter would be statistically expected if the standard error of estimate for each device (±1.95 nuclear and 2.33 balloon, as obtained from data shown in Figure 16 taken from a previous study (1) for the convenience of the reader) are considered in the calculations. The total estimate of error in calculations is equal to:

$$S_t^2 = S_n^2 + S_b^2 \qquad (1)$$

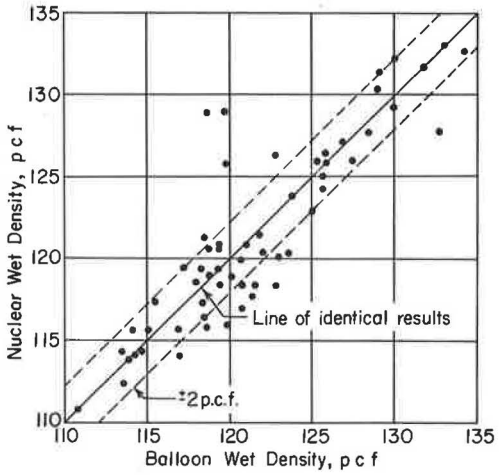

Figure 15. Results of field study, showing relationship between densities obtained by nuclear gage and by Rainhart balloon.

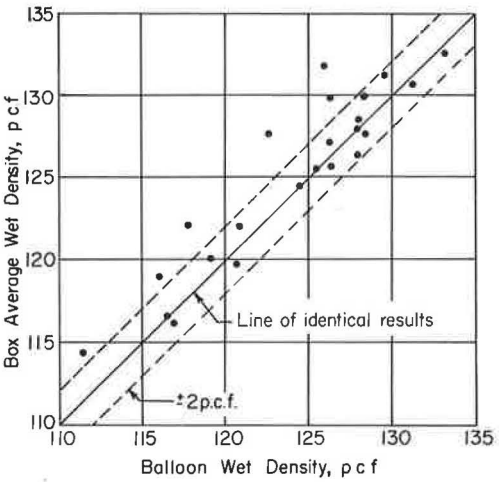

Figure 16. Results of previous study (1) in which density tests were conducted using Rainhart balloon on compacted samples.

TABLE 4

TIME COMPARISON STUDY

Test Method	Time (min)
Oil	28-30
Balloon	19-20
Nuclear	9-12

In this case S_t = ±3.04 pcf, and the computed total estimate of error using the data in Figure 15 is ±2.76 pcf. Since any variation greater than that determined from Eq. 1 would be attributed to soil type, the soils encountered on the 12 field projects did not appear to influence the results.

Throughout this study, a limited amount of minor difficulties were encountered with the equipment. However, with the use of the operational manual, the simplicity of the modular construction made it possible to perform all necessary maintenance. A problem was encountered with the timing system and a great deal of the calibration and initial field work had to be done with the aid of a stopwatch. The timer on the scaler used in this study is mechanical. This scaler has since been replaced with one having an electromechanical timer. Thus far, no difficulty has been encountered with the newer timer.

Time Study

Table 4 gives the average time required to conduct an in-place density test by the conventional procedure and with the nuclear equipment.

Table 5 gives a time comparison of the nuclear equipment and the balloon method. Instead of using the standard procedure of digging the density hole, a coring device was used with the balloon device. This speeded up the balloon tests considerably.

The time study points out that the nuclear equipment does have an unquestionably great advantage of speed. To illustrate further, one technician was as-

TABLE 5

TIME COMPARISON STUDY

Location	No. Tests	Device	Time (min)
Proj. 1	13	Balloon[a]	165
	13	Nuclear	120
Proj. 2	17	Balloon[a]	185
	17	Nuclear	125
Proj. 3	10	Balloon[a]	95
	10	Nuclear	65

[a]Motorized coring device used to dig density holes.

signed to four construction projects with the nuclear equipment. The normal assignment would be a minimum of three density men. For a period of 1 wk, the technician maintained the density tests required for all four projects. The construction sites were not a great distance apart; nevertheless, a nuclear-equipped density man did replace three density men equipped with conventional equipment, including three pickup trucks.

Radiological Safety

A radiological survey indicated a need for additional lead shielding during storage and transportation of the equipment. Even though the radium-beryllium source is not under the control of the Atomic Energy Commission (AEC), the source should be treated with the same respect as cesium or cobalt. The equipment should be "leak tested" at least twice a year and survey meters are readily available. Film badges should always be worn by personnel using the equipment.

During this study, only one of the personnel film badges recorded any radiation exposure. The film badge was used over a period of 4 wk with an accumulation of 80 mr, which is only 20 percent of the allowable AEC dosage of 100 mr/wk.

This study indicates that the equipment, if used conscientiously and monitored by a good radiological safety program (leak test, survey meters and film badges), can be used without any radiological health hazard.

CONCLUSIONS

1. Throughout this study, the direct transmission-type nuclear density gage has proven to be more accurate and much faster than conventional methods.
2. Use of the direct transmission principle in a nuclear density gage seems to eliminate the necessity for several calibration curves. As shown in Figure 11, the final calibration of the density gage is a single calibration curve which is suitable for the various soils tested and independent of depth for depths of 3 in. or more.
3. The nuclear equipment has been an asset to the Division of Research. The density tests conducted by research personnel are usually made in troublesome areas where the contractor is having difficulty in obtaining the specified density and where conditions necessitate repeated density tests. The nuclear equipment with its inherent speed has provided a means whereby the once time-consuming task of repeated density tests is considerably reduced.
4. The data obtained in this study indicate that the direct transmission-type nuclear density gage is an answer to the present need for a method of test which will keep pace with the advancements made in the capacities and speed of earthmoving equipment and with the expanded construction program.

The nuclear equipment is not only an asset in controlling density testing, but also a useful tool for setting up compaction equipment schedules and procedures. The amount of coverage required by a given type of compaction equipment to obtain specified density for an entire job can be determined quickly from one test section, provided extensive moisture or material changes were not encountered.

REFERENCES

1. A Report of the Evaluation of Various Methods for Determining In-Place Density of Soils. Florida State Road Dept., Div. of Res., Res. Bull. No. 56-A, July 1962.
2. Evaluation of a Nuclear Density-Moisture Apparatus. Florida State Road Dept., Div. of Res., Res. Bull. No. 55, Feb. 1961.
3. Determining Moisture Contents of Limerock Bases Using the Speedy Moisture Testing Apparatus. Florida State Road Dept., Div. of Res., Res. Bull. No. 13, Oct. 13, 1958.

Development of Nuclear Density Tests for Hot Asphalt Pavement

WAYNE R. BROWN, Colorado Department of Highways

Development of a nondestructive test method for density measurements of hot asphalt concrete in the field using portable nuclear instrumentation is described. Also described are effects to utilize existing nuclear density probes designed for testing soil to measure the compacted density of hot asphalt pavement.

A prototype nuclear asphalt density probe was developed. After testing the prototype on test sections with densities from 110 to 144 pcf, a production model asphalt density probe was designed and built. Heat-resistant electronics allowed density tests to be performed on material ranging in temperature from cold to 300 F. Source type and strength, as well as source-to-detector geometry, were optimized so that depth of penetration was restricted to approximately 1¾ to 2 in., allowing testing of thin asphalt surface courses without base course influence. Comparison data and compaction growth curves from various roller patterns set in the field using the asphalt density probe are included. Test results were available within 2½ min after each roller pass.

•SINCE PROPER compaction of freshly laid hot asphalt concrete is very important in highway construction, it is equally important that field density tests be made as quickly and efficiently as possible. Present conventional test methods are excessively slow and tend to relegate test results to the postmortem class. By the time the specific gravity of a cooled asphalt concrete specimen has been determined, the section of pavement being tested has usually cooled to the point where additional compactive effort does little or no good should the test fail.

Recognizing this and the fact that there was no commercially available nuclear probe for density tests on hot asphalt, the Planning and Research Division of the Colorado Department of Highways agreed to purchase a prototype nuclear density probe from the Nuclear-Chicago Corp. The purpose of this new device was to determine the compacted density of freshly laid hot asphalt concrete surface courses in the field. Design criteria called for the probe to have an effective depth of measurement of 2 in.

The Materials Division was given the tasks of assisting in the development of the device from a practical usage standpoint and of correlating the nuclear results with existing conventional test methods. To expedite these two assignments, test sections of asphalt concrete were constructed at the Asphalt Paving Co. plant west of Denver near Golden, Colo. These test sections were constructed according to the following specifications:

Section A—¾-in. maximum size, 30 percent minus No. 4 sieve, 5.5 percent asphalt;
Section B—¾-in. maximum size, 60 percent minus No. 4 sieve, 6.0 percent asphalt; and
Section C—100 percent minus No. 4 sieve, 6.5 percent asphalt.

Paper sponsored by Special Committee on Nuclear Principles and Applications.

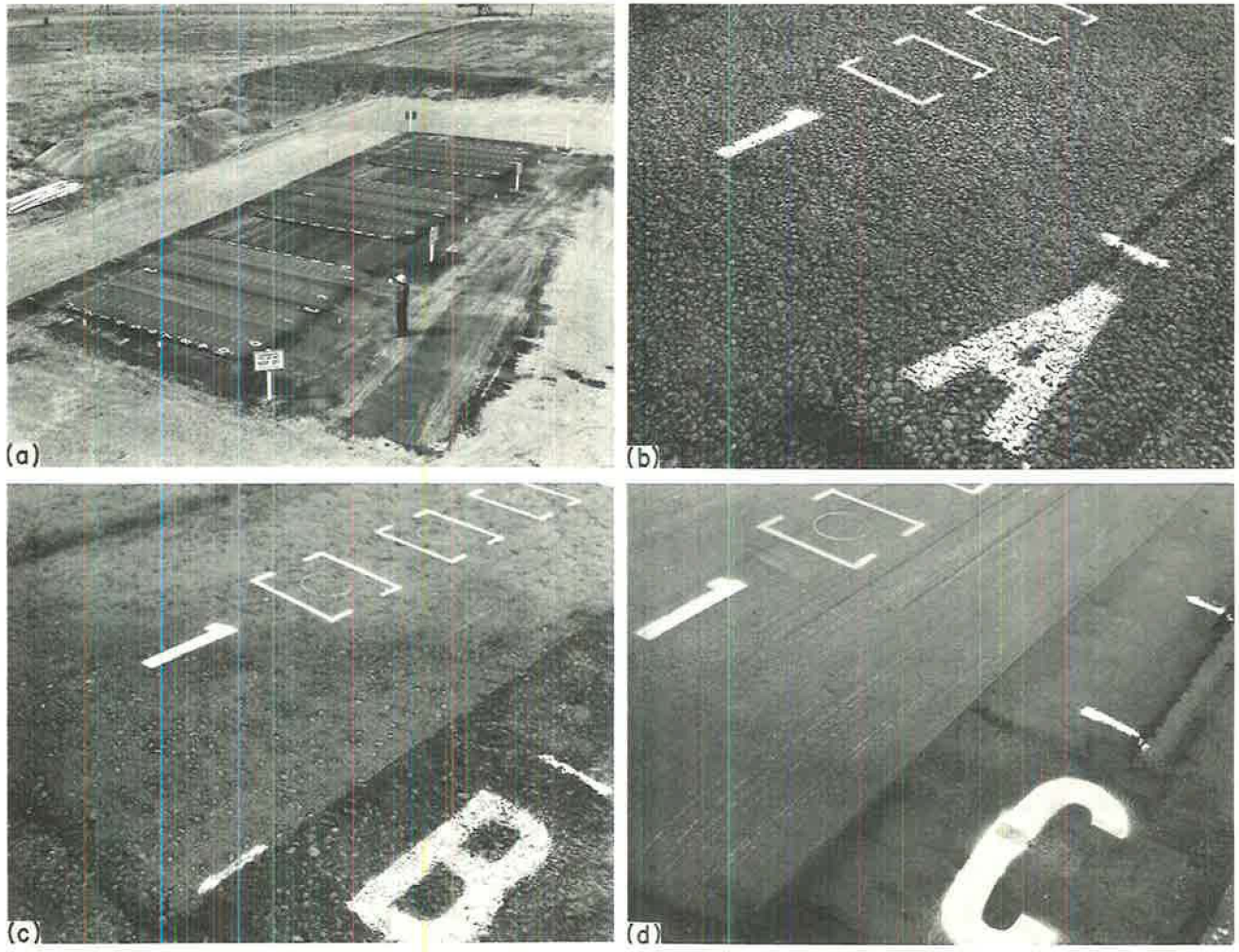

Figure 1. Asphalt test sections for nuclear testing program: (a) overall view; (b) closeup view of coarse-graded section; (c) closeup view of medium-graded section; and (d) closeup view of fine-graded section.

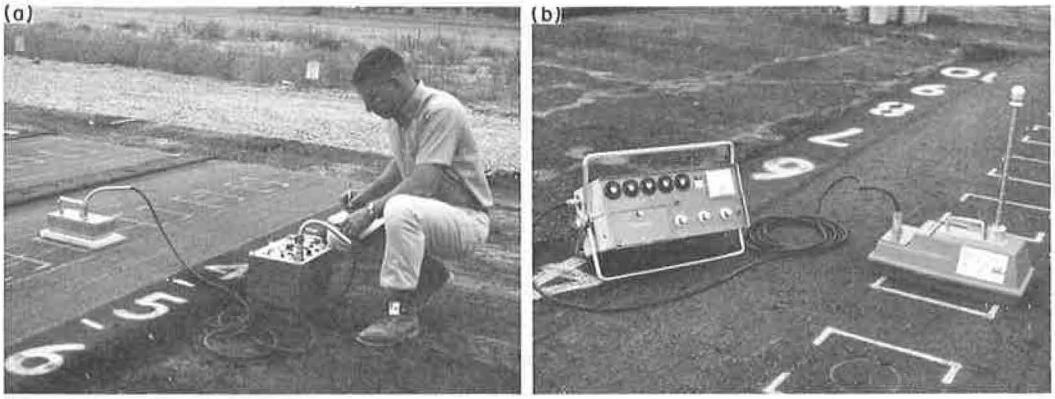

Figure 2. Density probes: (a) N-C Corp. P-22A on asbestos heat shield; and (b) Troxler being used on test sections.

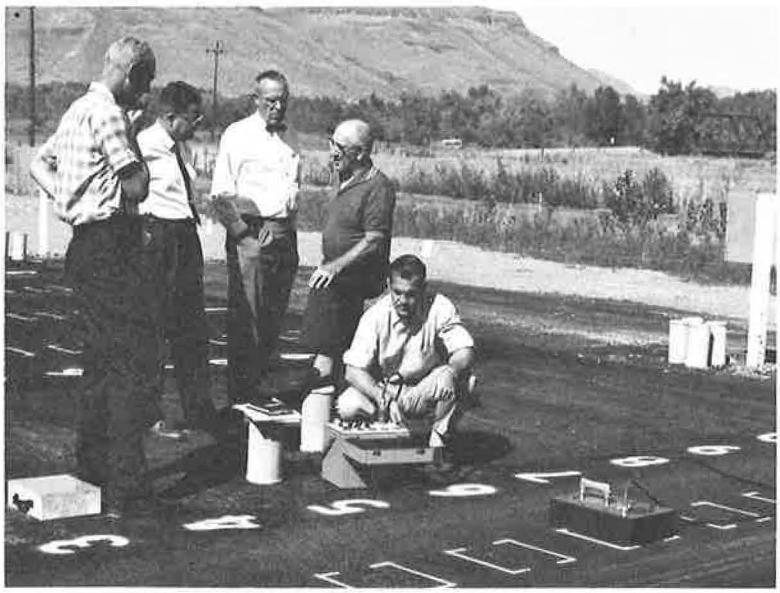

Figure 3. E-1-X prototype being operated on section B.

Each of these three sections measured 24 by 24 ft and were divided into four equal subsections (labeled 0, 1, 2, and 3). Subsection 0 had no compactive effort applied other than that of the vibrating screed at the rear of the SA-40 Barber-Greene paver. Subsections 1, 2, and 3 had roller passes applied that corresponded to these numbers. The roller used was a 10- to 14-ton Galion steel wheel tandem. Each of the subsections was then divided into 10 equal parts and indexed for testing as shown on Figure 1. This figure also includes closeup photos of each section illustrating the surface texture of the coarse, medium and fine mixes.

While waiting for the prototype to be developed, project personnel were instructed to log nuclear readings on the 120 indexed test sites using both the Nuclear-Chicago P-22 density probe with an asbestos heat shield (Marinite) (Fig. 2a) and the Troxler Model SC-120H surface density probe (Fig. 2b). The results of the tests using these two probes illustrated the need for developing a special probe for hot asphalt, since:

Figure 4. Polyethylene cover in place for weather protection.

Figure 5. Coring operation on test sections completed.

1. The slope of the calibration curve for the N-C Corp. P-22 was not steep enough to provide accurate readings;
2. The Troxler soil probe calibration curve had insufficient slope in the backscatter position, and
3. The Troxler soil probe could not be used in either the 1- or 2-in. position on hot asphalt because of the radiation hazard to the operator from wiping the source rod clean after each test.

The E-1-X prototype density probe was delivered to project personnel late in 1962 and nuclear readings were logged as weather would permit. Figure 3 shows the E-1-X being used on the test sections. A polyethylene cover was placed over the sections between test sequences involving the various nuclear devices so that moisture from rain or snow would not change the bulk density of the asphalt concrete (Fig. 4).

The E-1-X prototype consisted of a N-C Corp. P-22A with the six-tube detection system and the lower portion of the case removed. The remainder of the P-22 was placed in a relatively large case with appropriate lead shielding. The radioactive source of 3 millicuries (mc) of cesium 137 was changed to 2 mc of radium 226. A Transite heat shield was built into the bottom to protect the electronic components. The source-to-detector geometry had been selected experimentally by the N-C Corp. design engineers so that the effective depth of measurement under ordinary field conditions was held to approximately 2 in.

Field tests on asphalt concrete weighing 135 pcf and having a thickness of 2 in. showed that varying the underlying base material from 110 to 140 pcf had no appreciable

Figure 6. Specific gravity determinations in Central Laboratory.

effect on the count rate of the prototype. Laboratory tests on a specimen of asphalt concrete weighing 110 pcf indicated a difference of 2 pcf when varying the underlying base material from 119 to 152 pcf. These slight changes were considered tolerable at that stage of the prototype development.

A laboratory sample of asphalt concrete was heated to a temperature exceeding 250 F, and tests were performed on it while hot using the E-1-X prototype. No ill effects were noted because of the heat.

Coring of the 120 test sites within the test sections was accomplished subsequent to the logging of a total of 360 nuclear readings using the three probes previously mentioned. Figure 5 shows the test sections on completion of the coring. A Concore drill unit was employed using a 6-in. I.D. diamond-impregnated bit. The cores were wrapped in several feet of masking tape and placed in padded cartons. They were then transported to the CDH Central Laboratory and stored in a cool (unheated) room on a flat surface until the water from the coring operation had evaporated. Cores from the areas that had had no compactive effort applied were handled very carefully to prevent deformation of the sample.

Field trials involving the E-1-X showed that the new probe was quite sensitive to density after each roller pass. The electronic components were not affected by the heat of the mat, even though it exceeded 250 F.

A Dunagan apparatus was used to determine the specific gravity of the cores from the test sections. Standard procedure for Colorado Departments of Highways field personnel performing routine control tests was used. This method involves weighing of the uncoated specimen in air and in water and calculating the specific gravity (Fig. 6).

Representative core samples (eight from each section) were selected to be coated with paraffin to determine their density according to AASHO Test Method T-166-60. Table 1 gives the results using these two methods on cores from sections A, B, C, and E. (Section E is described later in this text.)

Significant differences in the results of the two methods appear, especially when the more porous cores are tested. From past experience, project personnel have learned that the acceptance or the rejection of a new concept of testing by field forces is always based on correlation obtained with standard field procedure. Therefore, since project personnel entered into this research project with the intent of assisting in the development of procedures for the CDH field use of an asphalt density probe, they are of the

TABLE 1

SPECIFIC GRAVITY OF UNCOATED VS PARAFFIN-COATED[a] CORES

Core No.[b]	Density (pcf)		
	Uncoated	Coated	Diff.
A-0-3	137.7	133.3	4.4
A-0-8	139.6	—	—[c]
A-1-3	140.2	135.8	4.4
A-1-8	143.3	—	—[c]
A-2-3	142.0	137.1	4.9
A-2-8	142.0	137.1	4.9
A-3-3	142.0	137.1	4.3
A-3-8	141.4	136.4	5.0
B-0-3	127.7	124.0	3.7
B-0-8	127.7	122.7	5.0
B-1-3	131.5	128.3	3.2
B-1-8	131.5	129.6	1.9
B-2-3	130.2	127.7	2.5
B-2-8	130.2	129.0	1.2
B-3-3	132.1	129.6	2.5
B-3-8	132.7	131.5	1.2
C-0-3	105.7	105.3	0.4
C-0-8	107.8	106.5	1.3
C-1-3	110.9	109.6	1.3
C-1-8	110.2	109.6	0.6
C-2-3	114.0	112.1	1.9
C-2-8	111.5	110.9	0.6
C-3-3	116.5	115.3	1.2
C-3-8	112.1	112.1	0.0
E-0-1	136.4	126.5	9.9
E-0-2	136.4	126.5	9.9
E-2-1	139.6	135.8	3.8
E-2-2	139.6	135.8	3.8
E-4-1	140.8	136.4	4.4
E-4-2	138.9	135.8	3.1
E-6-1	140.2	137.1	3.1
E-6-2	140.2	135.8	4.4

[a]AASHO Test Method T-166-60.
[b]Cores from sections A, B, and C were dipped in paraffin; section E cores had paraffin painted on.
[c]Specimen broke up when dipped in hot paraffin.

opinion that the CDH field testing procedure (uncoated specimens) should be the comparison criterion.

Figure 7 illustrates the correlation between the E-1-X prototype and conventional density determinations according to the specific gravity of the uncoated specimens. This chart illustrates the following:

1. Using the N-C Corp. calibration curve that accompanied the E-1-X, the nuclear results will be excessively low.
2. Using the CDH calibration curve (based on a least squares analysis of the section B and C core densities on cores having a thickness of $1\frac{3}{4}$ in. or more), 87 percent of the tests are within ±3 pcf of a common curve.
3. The section B core data falling out of tolerance to the right of the CDH curve came from an uncompacted area. Since routine field tests for relative compaction will not be taken in an area such as this, the deviation shown is not as significant as would appear at first glance.
4. The nuclear readings were affected by the base course material when areas tested had a thickness of less than $1\frac{3}{4}$ in. This is close to the 2-in. depth of penetration for which the prototype was designed.
5. Data from the very coarse Section A (30 percent minus No. 4) indicate that the nuclear readings are significantly affected by the excessive surface air voids and a calibration curve is unobtainable for this section. This is of no great concern to project personnel because, although CDH standard specifications encompass this type of mat, it is never constructed in Colorado.

The Model E-1-X prototype was then sent back to the N-C Corp. with a list of suggestions for design modifications for the production model density probe. These suggestions included the following:

1. A high temperature, infinite counting time, thin-wall Geiger-Müller tube similar to that being developed by the Amperex Company should be considered as the detector;
2. A detector tube having a reasonably flat voltage plateau should be incorporated in the production model;
3. The screened vent should be eliminated; and
4. The case should be elongated to permit easier seating.

In June 1963, a production model of the asphalt density probe (designated Model 5846) was delivered to project personnel. This probe (Fig. 8) is compatible with the Model 2800A scaler used to operate the other N-C Corp. portable nuclear probes.

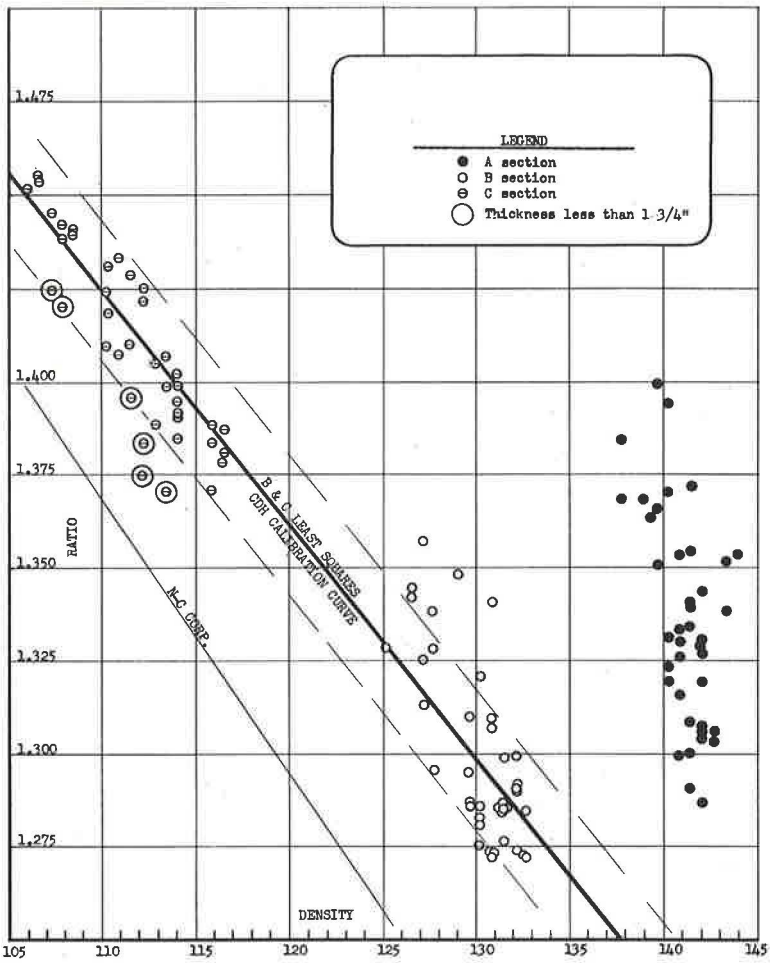

Figure 7. Correlation of conventional density determinations on sections A, B, and C with E-1-X prototype density probe determinations.

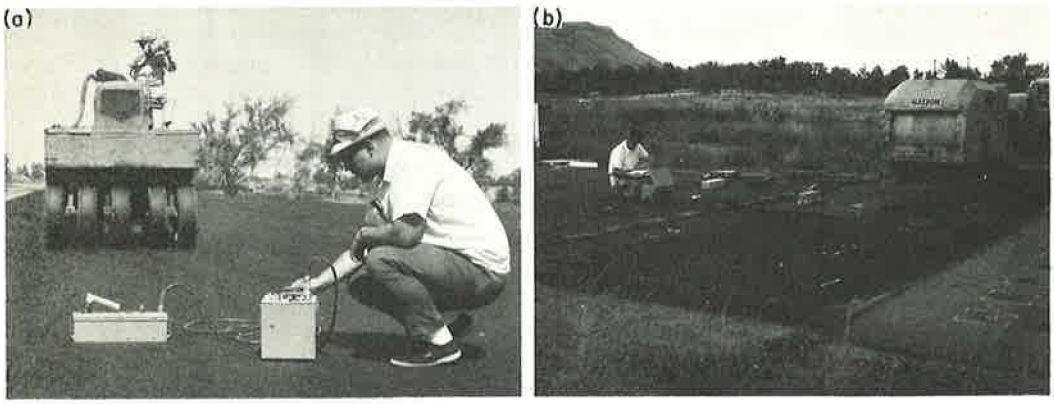

Figure 8. Model 5846 asphalt density probe: (a) being used in field trial; and (b) being operated on section E.

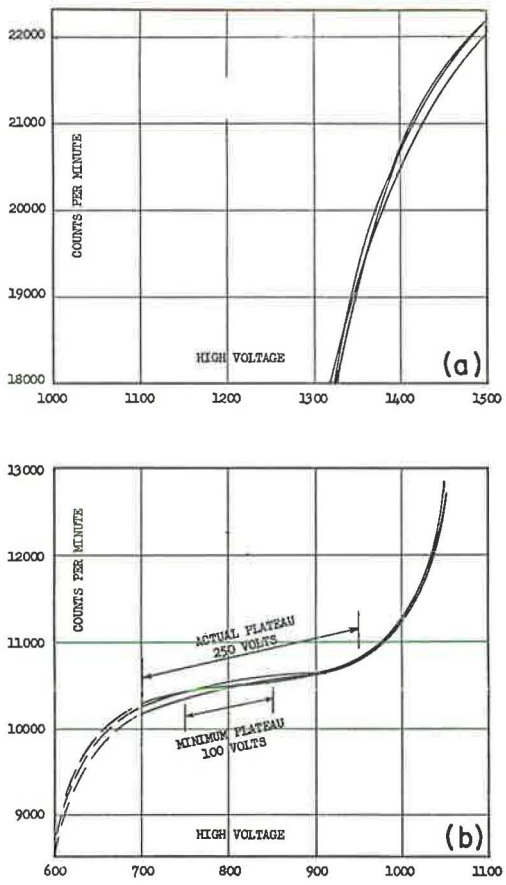

Figure 9. High-voltage plateaus: (a) E-1-X, and (b) Model 5486.

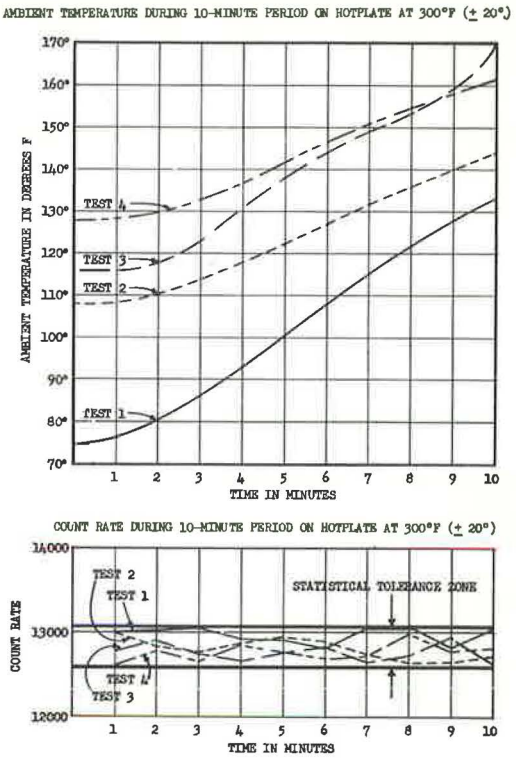

Figure 10. Model 5846 ambient temperature test results, series III.

The Model 5846 has incorporated into its design all the suggestions that CDH project personnel forwarded with the return of the E-1-X prototype. The first phase of laboratory tests involving the Model 5846 concerned the characteristics and the reproducibility of the high-voltage plateau of the new Amperex detector tube. Figure 9a illustrates the unacceptable curvilinear plateaus of the E-1-X. Figure 9b shows the excellent, reasonably flat high-voltage plateau of the Model 5846. The E-1-X has had this type of detector tube installed and now has a high-voltage plateau similar to that of the Model 5846.

The next phase of laboratory tests involving the Model 5846 pertained to a series of ambient temperature tests. Results of the last of a series of these tests, shown in Figure 10, indicate that this probe is not affected by heat up to 300 F originating from the material being tested.

The Model 5846 was operated on the test sections 1 ft to the east of the holes made by the core drill at the 120 test sites. Results of the tests were similar to the data shown in Figure 7. The data are available from the Colorado Department of Highways as a supplement to this paper.

The Model 5846 has been used in the field in Colorado to control the compaction of hot asphalt concrete surface courses. Figures 13 and 14 illustrate the field control results on hot asphalt on the Clifton-Cameo project. The new probe has also been used in Denver, Burlington, and on the Wolcott-North project to set roller patterns.

Acceptance of this new technique by both CDH and contractor personnel in the field has been good. CDH District VI (Denver) now has a Model 5846 probe that is being used for routine compaction control of hot asphalt and for setting roller patterns efficiently. CDH District III (Grand Junction) has a Model 5846 on order and plans to use it as an accessory to the density-moisture gages they now have in the field.

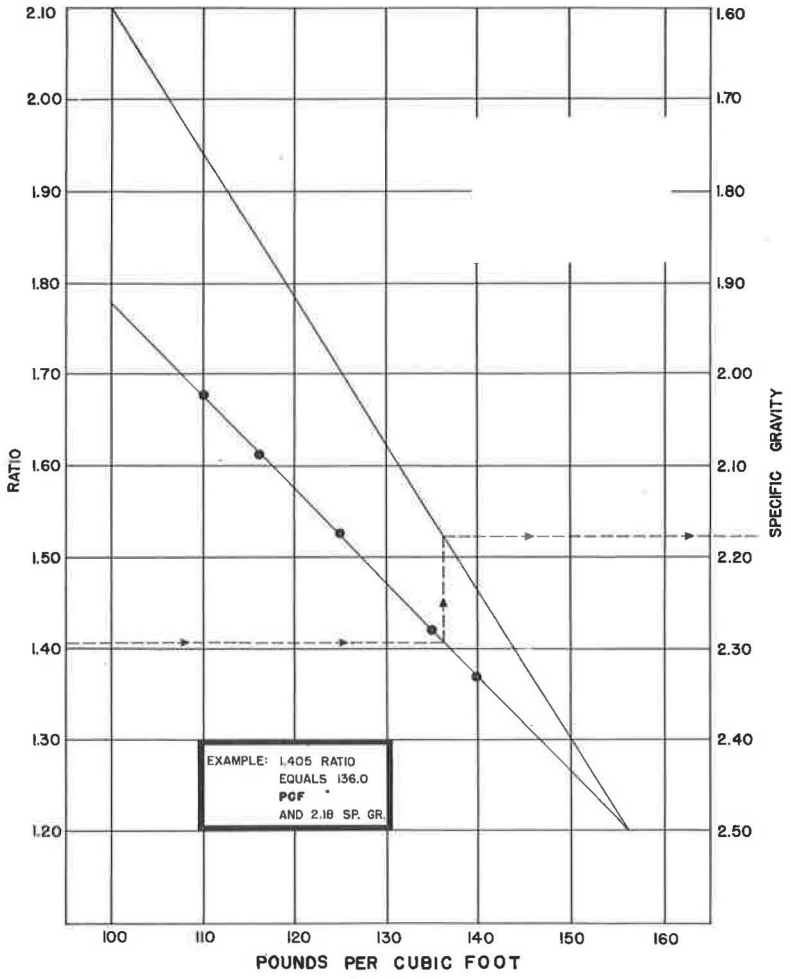

Figure 11. Model 5846 calibration and specific gravity conversion curves.

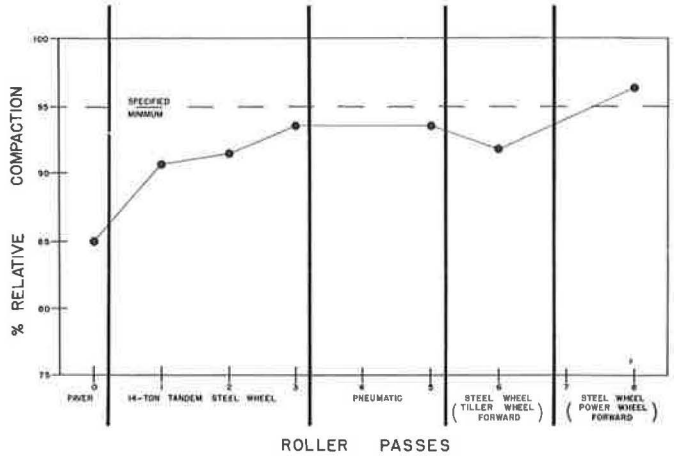

Figure 12. Compaction growth curve using Model 5846 nuclear density probe; Project I 70-4(26), E. 46th Ave.-Elizabeth St. to Jackson St. in Denver.

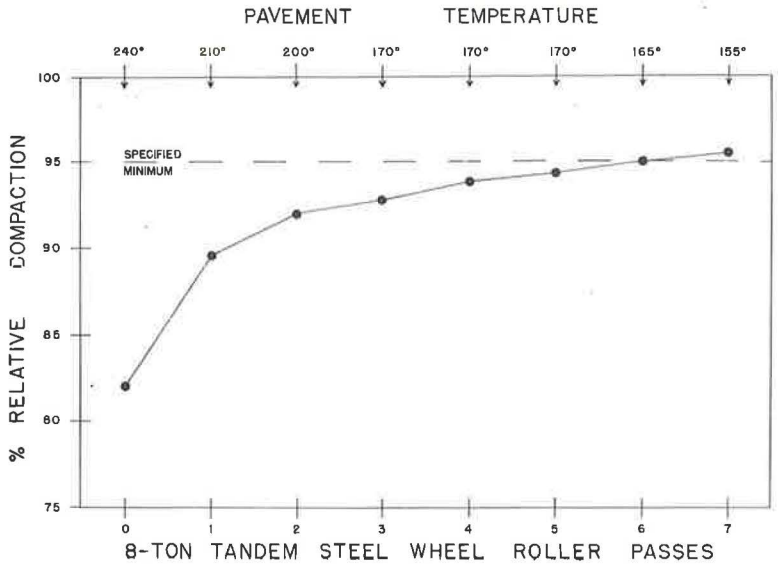

Figure 13. Compaction growth curve using Model 5846 nuclear density probe; Project I 70-1(7), Clifton-Cameo.

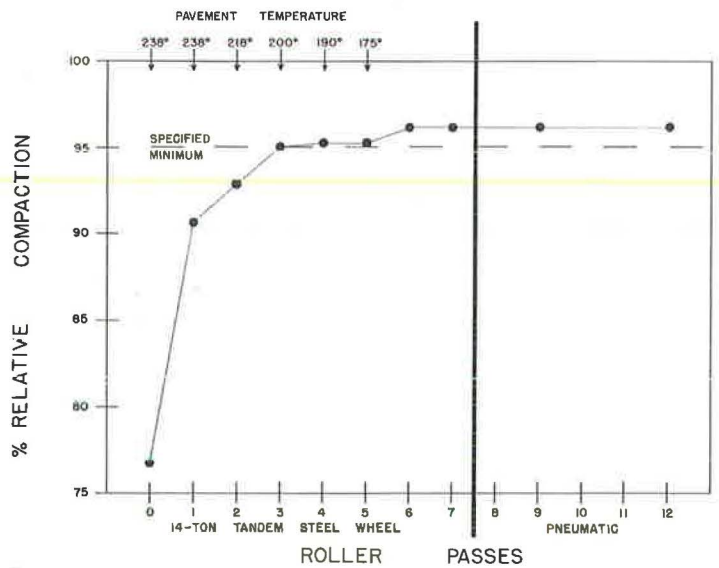

Figure 14. Compaction growth curve using Model 5846 nuclear density probe; Project I 70-1(7), Clifton-Cameo.

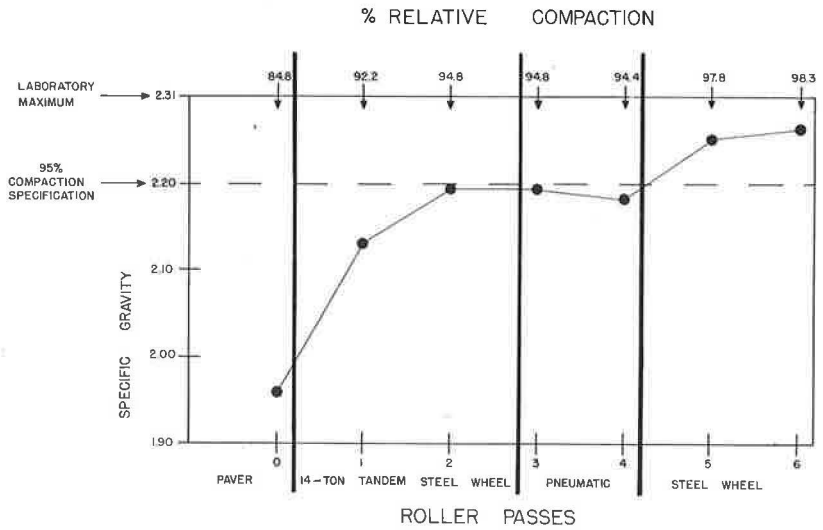

Figure 15. Compaction growth curve using Model 5846 nuclear density probe; Project U 012-2(9).

The Nuclear-Chicago Corp. has not supplied CDH project personnel with usable calibration curves for either the prototype or the Model 5846. The curves supplied were based on the company soil and concrete standards and were intended to be temporary, pending the completion of N-C Corp. asphalt standards of correct size, weight and uniformity.

CDH calibration standards compacted by hand in the Central Laboratory proved to be too small and nonuniform. Calibration standards being used at present were cut from the test sections with a diamond blade concrete saw. They measure 12 by 24 in. and are preserved in the Central Laboratory. Figure 11 shows the calibration curve for a Model 5846 based on these standards, as well as the specific gravity conversion curve for use in the field. The latter curve is useful because all data sent to the CDH field crews concerning laboratory maximum density for asphalt concrete are in terms of specific gravity.

To obtain a relatively high density area for a calibration standard, new sections of asphalt concrete (labeled D and E) were constructed in the space between the original three sections. Figure 8b shows Model 5846 being operated on section E. Specifications for these new sections were as follows:

Section D—¾-in. maximum size, 60 percent minus No. 4 sieve, 6.0 percent asphalt; and

Section E—¾-in. maximum size, 45 percent minus No. 4 sieve, 6.0 percent asphalt.

Roller passes on these sections varied from 0 to 12 passes of a 14-ton steel wheel roller. Maximum density obtained was 141 pcf and provided the necessary high density calibration standard.

Figures 12 through 15 show compaction growth curves developed in the field using the Model 5846 probe. These curves illustrate how readily a roller pattern may be established using the nuclear method, especially since each test takes less than 5 min to perform. These curves also show that pneumatic rolling has virtually no effect on pavement density after at least three passes of the steel wheel breakdown roller.

CONCLUSIONS

1. Nuclear density tests for hot asphalt surface courses are possible and practical during compaction.

2. Asphalt concrete temperatures up to 300 F may be tolerated during testing.
3. The effective zone of influence of the production model probe described in this paper has been arbitrarily set at 1¾ to 2 in. deep.
4. Nuclear results do not correlate well with conventional results on open-graded mixes having a significant amount of surface air voids.
5. Nuclear results correlate reasonably well with conventional results when testing the closer graded mixes used by the Colorado Department of Highways.
6. The nuclear method is preferable to the conventional method because (a) the complete nuclear density test is accomplished in less than 5 min, whereas the conventional test takes much longer; (b) the nuclear test is performed on the asphalt while it is still hot, thus allowing additional compactive effort to be applied while the asphalt is still hot should the test fail; (c) roller patterns are quickly set using the nuclear probe; (d) overrolling of asphalt pavements may readily be determined and corrected using the nuclear method, thus saving the contractor time and money should he be working under end-result specifications; and (e) the nuclear method is nondestructive.

Aggregate Production with Nuclear Explosives

SPENST M. HANSEN and JOHN TOMAN, University of California, Lawrence Radiation Laboratory, Livermore, California

•THE DEVELOPMENT of nuclear explosives in recent years has made available a new, cheap, and powerful energy source. Project Plowshare is a research program to develop industrial and nonmilitary applications of nuclear explosive energy. The technical investigations are conducted by the University of California Lawrence Radiation Laboratory, Livermore, and sponsored by the U. S. Atomic Energy Commission.

Underground experiments in hard rock have established the rock-breaking capabilities of nuclear explosions and have provided pertinent effects data. Breaking rock for the manufacture of crushed stone aggregate is an obvious application, and one within the present technical capability of Plowshare.

EFFECTS OF UNDERGROUND NUCLEAR EXPLOSIONS IN ROCK

Figure 1 summarizes the gross effects from underground nuclear explosions at various depths of burial for a given yield. The greatest potential for aggregate production exists at depths of burst deeper than normally used for explosive excavation (Fig. 1b).

Formation, description, and phenomenology of nuclear explosion craters and cylindrical chimneys of broken rock from contained nuclear explosions are described elsewhere (see References) and will not be repeated here except as relevant to aggregate production. Experiments in rock which directly relate to aggregate production include seven chemical and seven nuclear explosions. Essential data from these are summarized in Appendices A and B.

Tonnage of Rock Broken

Results of underground and cratering explosion experiments in rock have provided tonnage data as a function of yield and depth of burst, and are the basis for the family of curves shown in Figure 2. These curves permit the prediction of broken rock tonnage as a function of explosion yield and depth of burst. Specific curves are dependent on rock physical and chemical properties and will vary somewhat for different rock types.

From the shape of the curves, it is clear that for each explosion yield there is a depth of burial at which the maximum of broken rock can be produced. For hard rock the scaled depth of burst for optimum rock breaking is slightly greater than 200 $ft/kt^{1/3.4}$:

$$Dob' = Dob/W^{1/3.4} \quad (1)$$

where Dob′ is scaled depth of burst, Dob is depth of burst of explosive in feet, and W is yield of explosion in kilotons (kt).

Experimental Results Pertinent to Aggregate Production

1. Pre-Schooner Charlie.—The Pre-Schooner Charlie experiment, at a scaled depth of burst of 210, produced a pile of rock resembling a crater entirely above the original ground surface. The other Pre-Schooner experiments, Alfa, Bravo, and

Paper sponsored by Special Committee on Nuclear Principles and Applications.

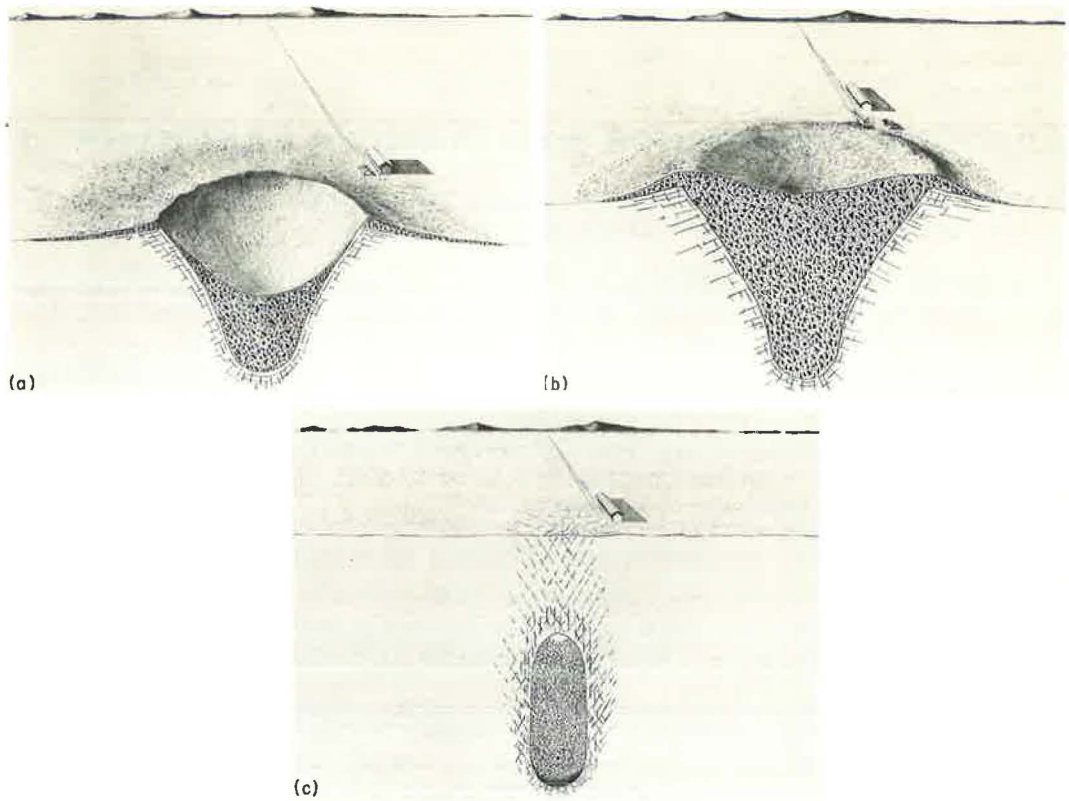

Figure 1. Effects of nuclear explosives buried at various depths: (a) optimum cratering depth $\left(\text{scaled Dob of } 140 \text{ ft/kt}^{1/3.4}\right)$; (b) maximum rock breakage depth $\left(\text{scaled Dob of } 210 \text{ ft/kt}^{1/3.4}\right)$; and (c) containment depth (scaled with 300-ft buffer overlying top of rubber column).

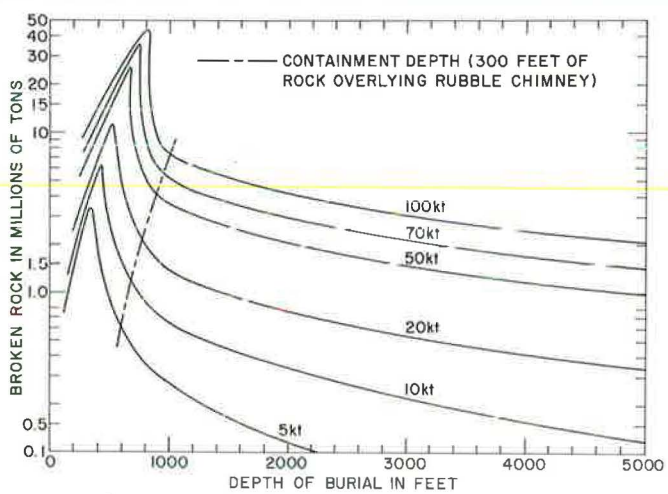

Figure 2. Tonnage curves of rock broken by underground explosions.

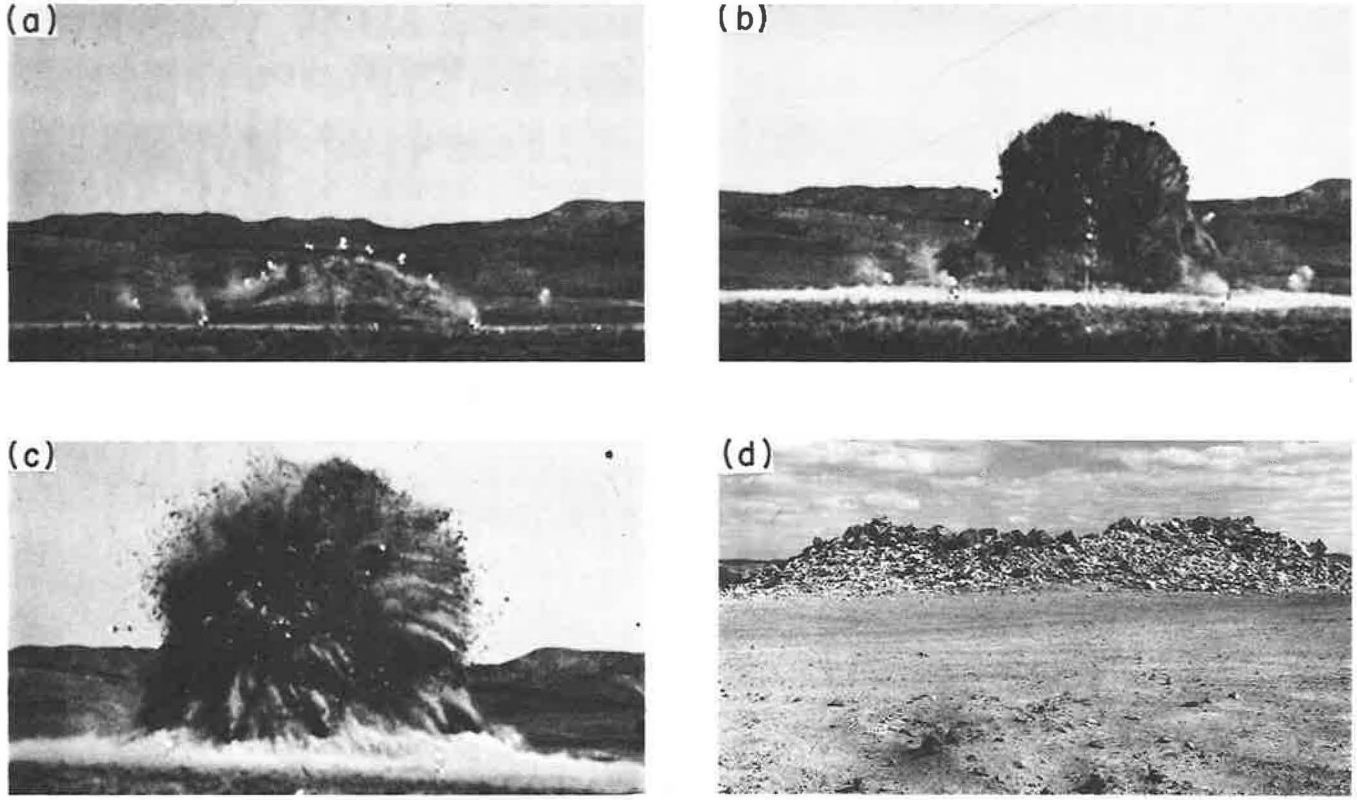

Figure 3. Pre-Schooner Charlie time-explosion sequence photographs: (a) 0.40 sec, (b) 1.20 sec, (c) 3.2 sec, and (d) postshot.

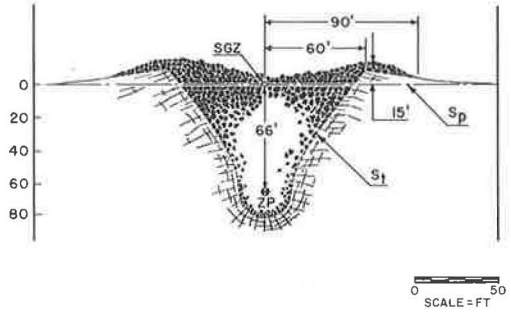

Figure 4. Schematic cross-section of Pre-Schooner Charlie crater.

Delta, which were buried at shallower depths, formed normal craters with a depression extending beneath the original ground surface. The Pre-Schooner Charlie explosion shattered the overlying rock and imparted sufficient velocity to hurl rock upward nearly vertically from the true crater (Fig. 3). The resultant rubble mound consists of fallback of explosion-broken rock. The increased volume of the rubble results from the increase in bulk of broken rock as compared to pre-explosion rock. Figure 4 is a preliminary cross-section through the Charlie experiment showing the true crater boundary and contained mass of broken rock.

Pre-explosion in-situ density was about 165 pcf. Estimates of bulk density of the rubble are about 100 pcf, giving a swell factor of approximately 1.6. Swell factor (S), used here as equivalent to the sometimes used bulking factor, is defined as the ratio of in-situ bulk density (D_i) to final bulk density of the rubble (D_r), or $S = D_i/D_r$. Swell factor may also be defined as the ratio of final postshot volume (V_f) to in-situ volume (V_i), or $S = V_f/V_i$. Estimates of bulk density and swell factor for the rubble produced by the Pre-Schooner Charlie explosion are based on data obtained by the Nuclear Cratering Group, U. S. Army Corps of Engineers, from the excavation of the Pre-Schooner Delta Crater (8) and on field observations by the authors.

2. Neptune.—The Neptune experiment was conducted at Rainer Mesa, Nevada Test Site, on a hillside with an average slope of 27 deg and at a scaled depth of burst of 189, measured normal to the average preshot slope. A cross-section of the Neptune crater is shown in Figure 5. Virtually all of the rubble ejected, plus additional slide material, was concentrated at the downhill edge of the crater and in a slide which terminated about 800 ft down the slope. No lip developed on the uphill side of the crater, but well-defined lips were formed along the sides. Neptune was fired at somewhat less than the scaled depth of burst for maximum rock breakage.

3. Danny Boy.—The Danny Boy nuclear cratering experiment (0.42 kt) conducted in basalt at the Nevada Test Site (18) yielded at least 100,000 cu yd of rock rubble and produced a crater (Fig. 6) approximately 214 ft across and 62 ft deep, measured at the preshot ground surface. The scaled depth of burst of 142 was about correct for optimum crater size. The explosion did not break as much rock as it would have with deeper burial.

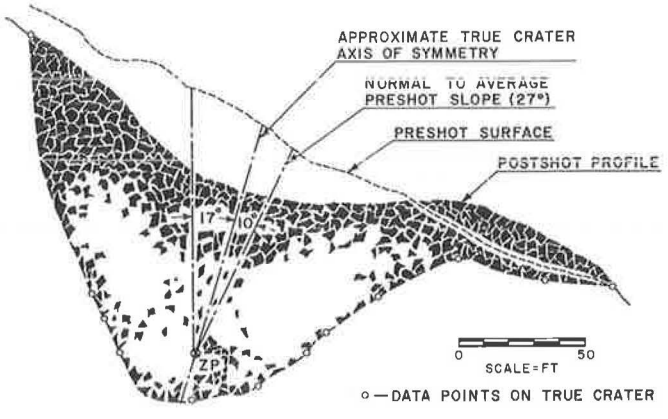

Figure 5. Schematic cross-section of Neptune crater.

Figure 6. View across Danny Boy crater showing general nature of explosion-broken rock (note man standing at upper center of photograph).

Figure 7. Rubble mound (diameter of approximately 164 ft) produced by Sulky explosion.

Figure 8. Edge of rubble mound formed by Sulky explosion.

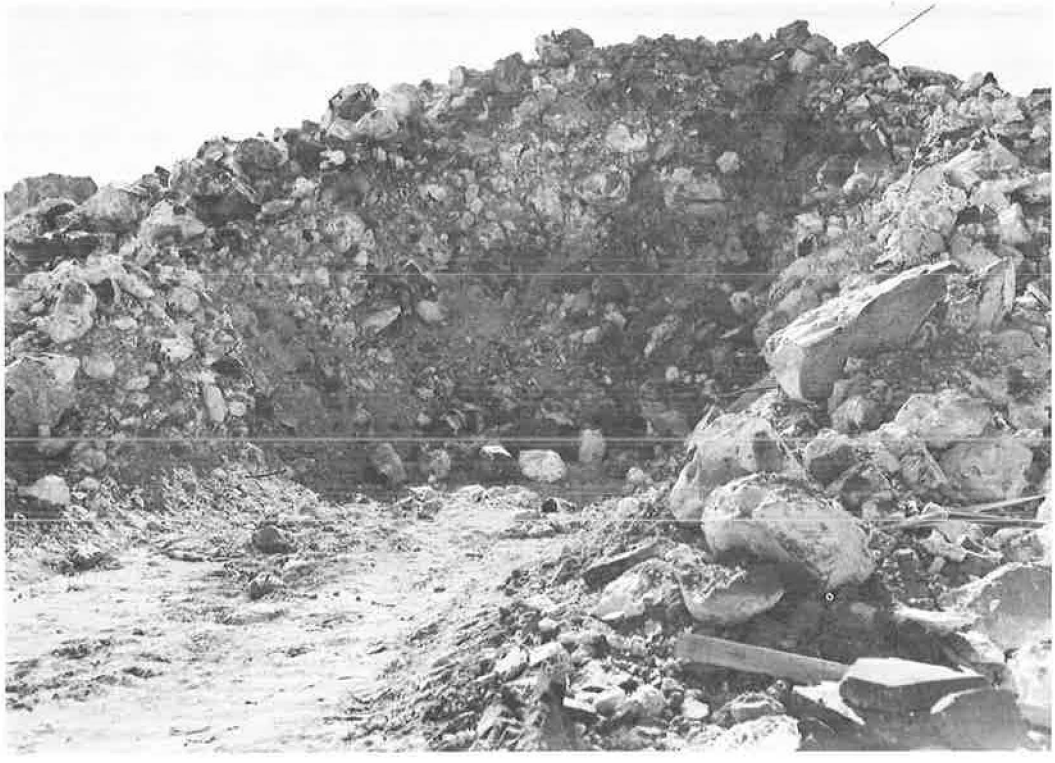

Figure 9. Trench cut partially into Sulky rubble mound, showing size distribution of rock fragments; vertical bank approximately 25 ft high.

Rock size distribution data obtained by screening an 800-ton sample obtained from the crater lip indicates that the rubble produced by the explosion would be suitable for use as aggregate after sizing and/or crushing to meet standard specifications. A 200- to 400-ton/hr crusher, capable of accepting rock up to 28 by 40 in. in size, could handle at least 70 percent of all explosion-broken rock without secondary blasting. The Danny Boy experiment also provided data that established the relationship between pre-explosion joint and fracture frequency and rock fragment size.

4. Sulky.—The Sulky nuclear explosion experiment took place on Buckboard Mesa, Nevada Test Site, on Dec. 18, 1964. The explosion was detonated in hard dry basalt at a depth of about 90 ft. The approximate yield of the explosion was the equivalent of 87 tons of TNT.

A mound of rubble was formed (Figs. 7 and 8) with a maximum height of about 25 ft above the preshot ground surface and a diameter of over 160 ft. The explosive in the Sulky experiment appears to have been buried slightly too deep for maximum rock breakage, in spite of its calculated scaled depth of burst of 184. This is believed to have resulted from difficulties in scaling to very small nuclear explosive yields and from the low content of gas-forming constituents (water and carbonate) in the basalt medium. Radiation levels were sufficiently low that personnel were able to move freely about the rubble mound within a few days, and excavation of trenches and removal of broken rock began within a month. Trenches were cut by the U. S. Army Corps of Engineers with an International TD-25 bulldozer along radial lines into the mound. Figure 9 shows one of these trenches.

Fragment Size Distribution of Broken Rock

Factors that influence the overall rubble size distribution and maximum rock fragment size and shape include: (a) characteristics and frequency of natural fractures, (b) physical properties of the in-situ rock, (c) explosion yield, and (d) depth of burial. Typical fragment sizes based on data obtained by the U. S. Army Corps of Engineers from the Danny Boy and Pre-Schooner experiments in basalt on Buckboard Mesa, and on Lawrence Radiation Laboratory data from the Hardhat experiment in granite, are as follows:

Passing 6-ft sieve, 100 percent;
Passing 5-ft sieve, 95 percent;
Passing 4-ft sieve, 88 percent;
Passing 3-ft sieve, 75 percent;
Passing 2-ft sieve, 60 percent;
Passing 1-ft sieve, 40 percent;
Passing 6-in. sieve, 30 percent;
Passing 4-in. sieve, 25 percent;
Passing 2-in. sieve, 20 percent;
Passing 1- to ½-in. sieve, 16 percent;
Passing 1-in. sieve, 14 percent;
Passing ¾-in. sieve, 12 percent;
Passing ½-in. sieve, 10 percent;
Passing ⅜-in. sieve, 9 percent; and
Passing No. 4 sieve, 7 percent.

The distribution of preshot fractures, including the development of joint sets, is probably the most important single factor determining the final size distribution of explosion-broken rock. Fracture characteristics, such as lateral extent, amount of recementation, and spacing between break surfaces, are also significant. Fractures provide preferred sites for separation and/or breakage, and tend to limit the maximum dimensions of each rock fragment. Extensive subsurface geologic investigations of the Buckboard Mesa were conducted for the Pre-Schooner series. The U. S. Army Corps of Engineers reports that about 90 percent of the joints and natural fractures measured in vertical holes were closer than 5 ft and 50 percent were less than 1 ft (1, pp. 33-34). Explosion-broken basalt fragments on Buckboard Mesa usually show evidence of two or more sides of weathering and surface alteration, indicating these postshot fragment

boundaries were preshot fracture planes. Well-developed, but unseparated, natural fractures are seldom observed transecting postshot rock fragments.

Physical properties of rock in place, including crushing strength, shear strength and tensile strength, affect overall fragmentation and the formation of new fractures. Fragment size distribution differences between broken granodiorite (strong, hard crystalline rock) in the Hardhat experiment (2) and varieties of volcanic tuff (relatively soft, low crushing strength rock) in the Rainier experiment (24, 26) illustrate the effect of physical properties on size distribution of rubble.

At depths of burst in the cratering range and near the maximum for rock breakage, shattering of rock overlying the explosion and the upward velocity imparted are dependent on both yield and depth of burial. Impact breakage of rock fragments from downward fall is also dependent on these factors.

ENGINEERING CONSIDERATIONS

Production of crushed stone from nuclear aggregate quarries will require modified methods of quarry development and rock handling. In some instances, advantages of lower cost, greater versatility and reduced development lead time will result; in others, nuclear quarrying will be less advantageous than conventional methods, or will not be applicable at all.

The emplacement and detonation of a nuclear explosive at a suitable site can produce millions of tons of broken rock more quickly than can conventional means. This broken rock can be sized and utilized directly as rough aggregate, or it can be used as raw material for the manufacture of processed aggregate. The larger sized fragments might serve to advantage as riprap or anchor rock.

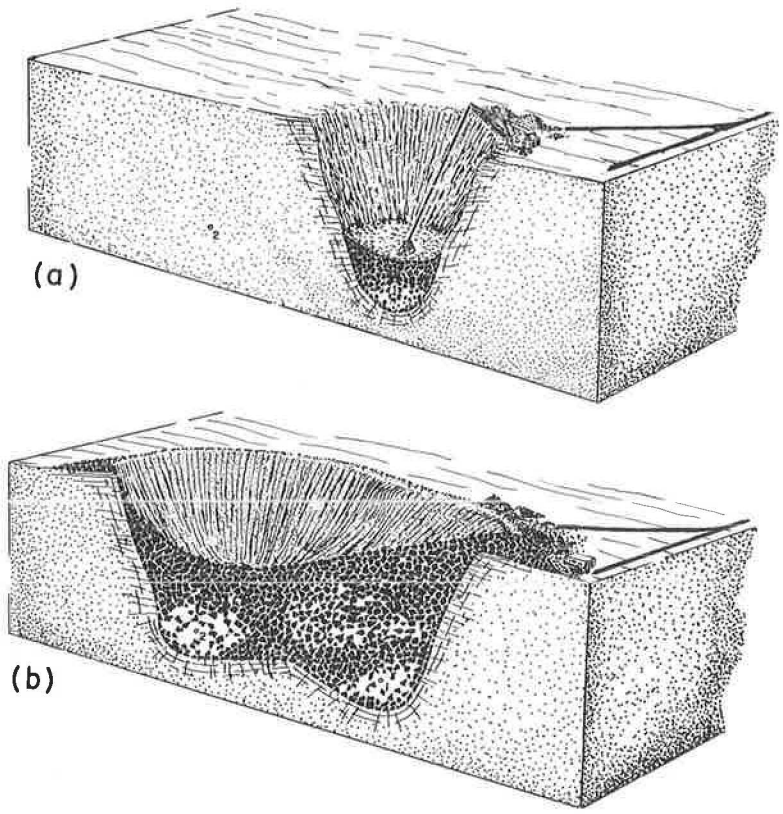

Figure 10. Multiple explosion quarry: (a) rubble mined out after first explosion, and (b) quarry after second explosion with rubble not yet mined.

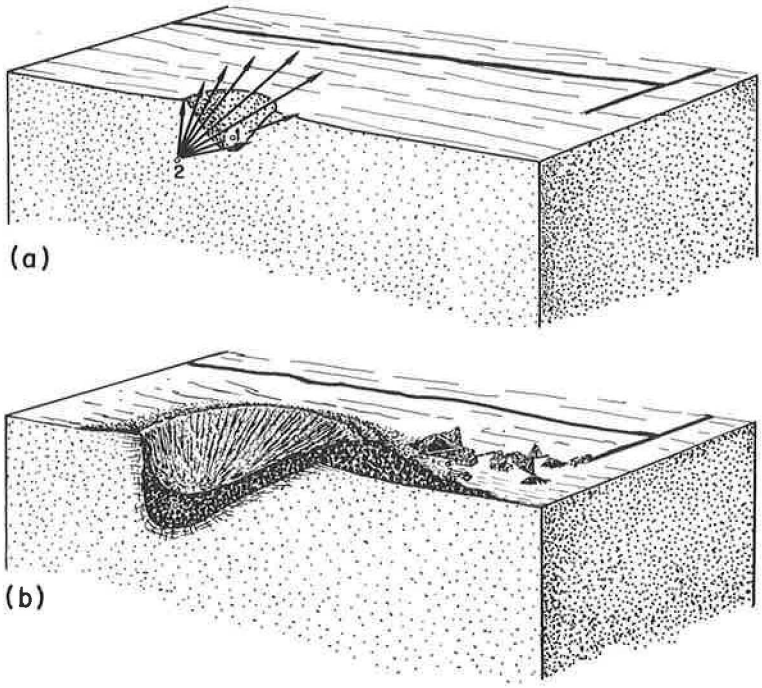

Figure 11. Aggregate quarry by directed nuclear explosion: (a) explosion placement and throwout zone; and (b) completed quarry showing location of ejected rubble.

Major engineering works, including dams, military installations, and interstate highways, are frequently located in areas remote from population centers and developed sources of aggregate. Nuclear aggregate quarrying might free such projects from construction delays caused by aggregate shortages, as well as from excessively high aggregate costs as a result of long hauls.

Site Selection

Sites suitable for the establishment of nuclear aggregate quarries will need to meet a number of requirements. Many of these are also requisite to conventional quarry development, and include: (a) the presence of rock with the desired chemical and physical properties, (b) minimum overburden or waste rock cover, (c) favorable topography, and (d) suitable natural fracture characteristics and fracture distribution. Nuclear quarry sites will also require greater thicknesses of suitable aggregate rock and will be restricted by safety problems arising from the use of nuclear explosives. The most important site limitations are expected to arise from possible seismic and shock damage to the surrounding area. Considerations of safety are briefly summarized in a later section.

Nuclear explosive quarrying techniques might make possible the use of sites where overburden or overlying rock cover prohibits the economic use of conventional explosives, and thus would relax this requirement for quarry site selection. This might be done by using nuclear explosives to strip off the overburden or by directed explosion quarrying (Fig. 7).

Quarry Layout

Several nuclear quarry designs have been considered and evaluated. Three approaches to nuclear aggregate quarry development on horizontal terrain that appear technically feasible are shown in Figures 10 and 11. The multiple explosion quarry

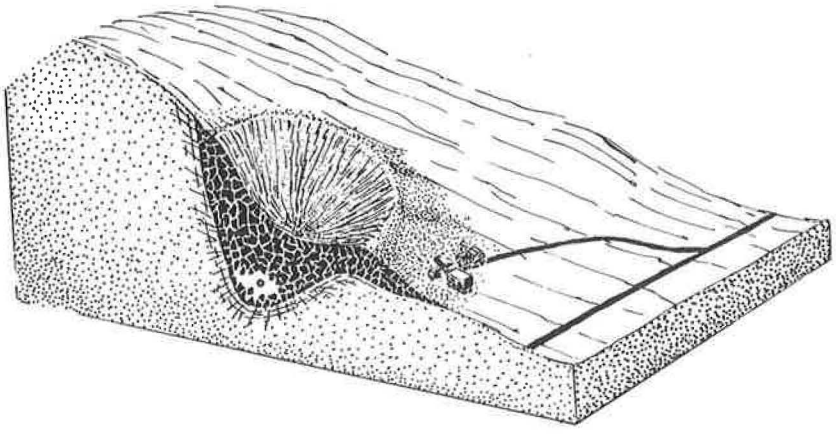

Figure 12. Aggregate quarry on a sidehill slope.

(Fig. 10b) is simply a follow-up modification of the single explosion quarry (Fig. 10a).

The directed explosion quarry is shown in Figure 11 (19). This approach utilizes a depression which could be formed by a smaller explosion buried at cratering depth, followed by a larger, more deeply buried explosion. The asymmetric placement of the larger explosion in relation to the depression causes the throwout to be directed as shown in Figure 11a. The final quarry shape, with the large mass of rubble expelled from the quarry, is shown in Figure 11b.

Explosions on a sidehill slope, buried at maximum rock-breaking depth, will produce more usable rubble for aggregate than will the same yield explosion on horizontal terrain. This is partly because gravity collapsed of the fractured zone on the uphill side of the crater adds to the total tonnage of rock broken. Also, a larger percentage of the rubble ends up outside the crater on the downhill side and rubble remaining inside the crater can be more easily removed by means of a trench cut in the downhill crater lip. The volume of rubble in the Neptune slide area alone is at least equivalent to the total volume of broken rock that would be expected from a comparable explosion at optimum cratering depth of burial on flat terrain. It is likely, therefore, that hillsides will offer preferred sites for nuclear aggregate quarries (Fig. 12).

Explosive Emplacement

Nuclear explosive packages can be emplaced by drill holes or underground drifting. At relatively shallow depths and with smaller diameter explosives, drill-hole emplacement from the surface offers cost advantages. In some instances, however, particularly when very large explosive packages are required, underground drift emplacement may be cheaper. Such a determination must be made on the basis of individual circumstances.

Standard equipment and excavation methods can likely be utilized to remove the broken rock, or new techniques might be developed. However, specific procedures can best be determined by those involved in aggregate production and marketing. A detailed discussion of this and of subsequent sizing, crushing, and other rock processing steps necessary for the production of marketable rough and processed aggregate is beyond the scope of this paper.

Because of the short time required to bring a nuclear aggregate quarry into production and the relatively small capital outlay which may be completely amortized on the basis of aggregate for a specific short-term project, long quarry life is not essential. Therefore, the aggregate source may be located close to the point of consumption, if a suitable site can be found. In such cases, considerations of long-term production and marketing will not be important factors in determining quarry location. Since aggregate is a high-bulk, low-unit value commodity, the cost of transportation becomes a

major factor in the total delivered aggregate price. On a per-ton basis, using the 1964 average market price for crushed stone of $1.42 at the quarry (28), a haulage of from approximately 20 to 30 mi at $0.05 to $0.08/ton-mi doubles the quarry price.

COST OF USING NUCLEAR EXPLOSIVES TO BREAK ROCK

AEC Charges for Nuclear Explosives

During May 1964, the U. S. Atomic Energy Commission published a revised schedule of charges for nuclear explosives (9). These charges include the explosive itself and its arming and firing, but do not include safety studies, site preparation, and costs of emplacement and support. The nuclear explosive charges are $350,000 for a 10-kt yield and $600,000 for a 2-megaton yield. Interpolations for intermediate yields are based on a straight line drawn between these two charges on semilogarithmic paper and are to be considered only approximations (Fig. 13).

The cost of energy on a per-unit basis from nuclear explosives is substantially lower than that from conventional explosives. The comparison is summarized in Table 1.

TABLE 1

APPROXIMATE COST OF EXPLOSIVE ENERGY

Explosive	$1 Million BTU's
TNT	115.00
Dynamite	100.00
Ammonium nitrate-fuel oil	30.00
Nuclear:	
10-kt	8.75
100-kt	1.12
1-megaton	0.145
2-megaton	0.075

Nuclear explosives can be designed to optimize particular characteristics such as explosive package size, cost, and radioactive by-products. Trade-offs between desirable properties often must be made in the selection of a nuclear explosive device for a project. Of particular interest for applications in aggregate production, as in many industrial applications, is the explosive package size. The minimum explosive sizes published by the Atomic Energy Commission are 10-kt yield with a cylindrical canister 12 in. in diameter for emplacement in a 13-in. I.D. drill hole and 100-kt yield with a cylindrical canister 18 in. in diameter for emplacement in a 19-in. I.D. drill hole. These minimum sizes do not necessarily

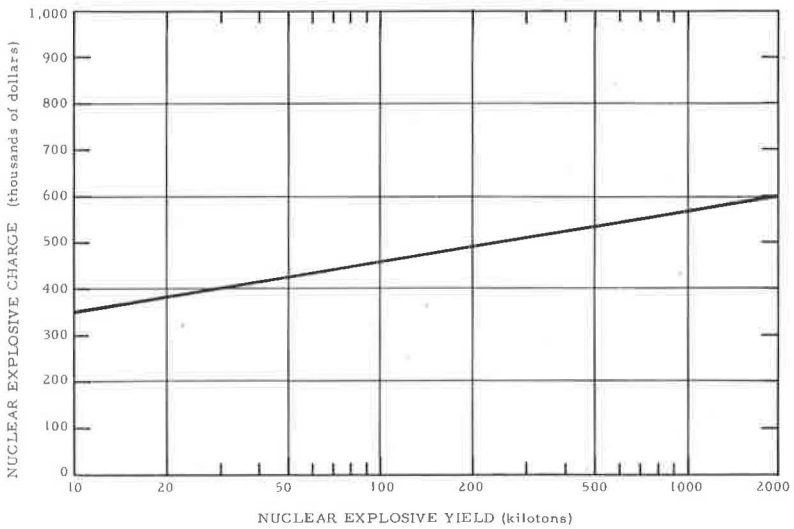

Figure 13. Projected charges for thermonuclear explosives.

TABLE 2

COST ESTIMATES FOR BREAKING ROCK WITH NUCLEAR EXPLOSIVES

Explosion Yield (kt)	Approx. Explosion Charge ($)	Million Tons of Rock Broken	Approx. Emplacement and Other Costs[a]	Total Costs ($)	Cost of Rock Broken ($/ton)
10	350,000	6 million	200,000	550,000	0.092
20	390,000	11 million	225,000	615,000	0.056
50	425,000	25 million	250,000	675,000	0.027
70	450,000	33 million	275,000	725,000	0.022
100	475,000	43 million	300,000	775,000	0.018

[a]Safety costs not included; must be evaluated separately for each individual site, and may be prohibitively high in some instances.

correspond to the nuclear explosive charge data summarized in Table 1, since charges for explosives with special characteristics, including minimum size, can be expected to be somewhat higher.

Per-Ton Costs of Breaking Rock with Nuclear Explosives

Cost estimates given in Table 2 are believed to be reasonable approximations for breaking rock with nuclear explosives for aggregate quarrying on a repeating, production-line basis. Included in these cost estimates are AEC charges for nuclear explosives and their arming and firing, emplacement and related engineering costs for site development, and support and other miscellaneous costs. Not included are the direct costs of safety studies and expenditures for the indemnification of any resultant postshot damage. Expenses resulting from considerations of safety vary greatly and are highly dependent on the specific project, the region in which it is carried out, and whether or not it is a single explosion or one of a series.

As may be noted, the per-ton cost of rock breakage with nuclear explosives is comparable to or lower than with conventional techniques. The advantage increases with the use of larger yield explosives. The cost estimates are only of breaking rock and do not include major items such as site acquisition, extracting rubble from the quarry, or any subsequent treatment necessary including crushing, sizing, screening, and washing.

SAFETY CONSIDERATIONS

Any use of nuclear explosives will require careful attention to problems of safety. To date, the Atomic Energy Commission and the Lawrence Radiation Laboratory have gained experience from the detonation of more than 100 nuclear explosives underground at the Nevada Test Site and elsewhere. Data gathered from these tests and from follow-up investigations have provided a basis for reliable preshot assessments of potential hazards from shock and radioactivity. Techniques have been developed for avoiding or minimizing most of these.

Shock and Seismic Effects

Experience from underground explosions, together with a theoretical understanding of pertinent phenomena, permits the reasonably accurate prediction of shock magnitude as a function of distance from the explosion. Table 3 gives a summary of damage categories based on peak surface velocity, a quantity found to be the most effective measure of shock damage (4). These data permit an estimate of the damage threshold distances for equipment and structures in the vicinity of a given shot. Variations in the wave form, seismic path, and particular structures add significant uncertainty to

TABLE 3

STRUCTURAL DAMAGE THRESHOLDS FOR BUILDINGS AND EQUIPMENT NEAR UNDERGROUND NUCLEAR EXPLOSIONS

Type of Structure	Type of Damage	Peak Surface Velocity Threshold, Major Damage (cm/sec)	Corresponding Scaled Distance in Granite[a] ($ft/kt^{1/3}$)
Residential (old)	Plaster cracking	10	2,500
Residential, concrete block	Cracking	20	1,250
Cased drill holes	Vertical displacement, horizontal offset	40-50	750-550
Mechanical equipment (pumps, compressors, generators, etc.)	Skids bent, shafts misaligned	100	375
Prefab metal buildings on concrete pads	Cracked pads, distorted steel	150	250
Rigid steel tanks, 50 gal to several thousand gallons	Buckling	≥300	125
Utility poles	Falling	≥300	125

[a]Distances are for structures resting directly on a hard crystalline rock such as granite, with the explosion detonated in the same medium, and do not include a safety factor. They are, therefore, a minimum and apply only to this ideal case. For most industrial applications, distances would probably be substantially increased (doubled or more) to provide a safety factor and to take into account possible presence of different and less favorable geologic conditions.

the values listed in Table 3. Prediction of damage will require the detailed evaluation of specific sites. Protection of personnel and portable equipment can be assured by moving them a safe distance from the detonation. Damage to stationary equipment and structures can be estimated before the shot, and the cost of the expected damage can be written off as a production cost.

Air blast is a major consideration for nuclear explosives at very shallow depths of burial or in the atmosphere. However, for shots buried at maximum rock-breakage depths, the zone of air blast damage can be expected to lie well inside the region of expected seismic damage.

Radioactivity

All nuclear explosives have some radioactive by-products. The amounts and types of activity are dependent on the energy yield and type of explosive. At the scaled depths of burst utilized for aggregate production, the venting to the atmosphere would carry only about 0.1 percent of the total fission radioactivity produced and would be a manageable hazard. Based on experience from the Danny Boy and Sulky experiments, a small amount of highly vesiculated rock melt with low specific radioactivity would be distributed throughout the rubble. The small amount of this material and its low level of radioactivity is not expected to be a hazard to personnel or to restrict in any way the utilization of the rock broken by the explosion.

In some instances it may be necessary for operating personnel to wear respirators or to take other standard precautions. However, the continued development of relatively clean nuclear explosives will tend to reduce even further the radioactivity safety problems encountered in the open-pit mining of aggregate.

The possibility of groundwater contamination by radioactive fission products has been extensively investigated. The radioactive materials trapped in solidified rock melt at the base of the original explosion cavity and distributed throughout the rubble will probably not cause serious groundwater contamination problems (23).

CONCLUSIONS

Breaking rock with nuclear explosives for use as rough aggregate or as raw material for the manufacture of processed aggregate is now technically feasible, as has been demonstrated by underground experiments in hard rock. Limitations arising from safety considerations are not excessive and will permit the use of nuclear explosives at many sites.

The greatest spur to the introduction of nuclear explosives as a tool for breaking rock in the multibillion-dollar aggregate-using industries will be the great potential for increasing the availability of high-quality crushed stone aggregate and doing so cheaply. Under favorable circumstances, the total per-unit cost of crushed stone from a nuclear explosion quarry, after sizing and all necessary processing, can be lower than the cost of a similar product produced by conventional methods.

Technical questions still remain to be answered in such areas as the use of multiple nuclear explosives and methods of removing broken rock from the nuclear explosion quarry. These will be solved in due course as commercial applications develop and industrial experience with nuclear aggregate quarrying is obtained.

REFERENCES

1. Banks, D. C., and Saucier, R. T. Geology of Buckboard Mesa. U. S. Army Engineer Waterways Exp. Sta., Vicksburg, Miss., PNE-5001, 1964. 147 pp.
2. Boardman, C. R., Rabb, D. D., and McArthur, R. D. Characteristic Effects of Contained Nuclear Explosions for Evaluation of Mining Applications. Lawrence Radiation Lab., UCRL-7350, 1963. 106 pp.
3. Butkovich, T. R., Calculation of the Shock Wave From an Underground Nuclear Explosion. In Engineering with Nuclear Explosives, pp. 35-50. Proc. 3rd Plowshare Symposium, U. S. AEC, Div. of Tech. Info., TID-7695, 1964.
4. Cauthen, L. J. Effects of Seismic Waves on Structures and Other Facilities. Lawrence Radiation Lab., UCRL-7773, 1964. 36 pp.
5. Circeo, L. J. Engineering Properties and Applications of Nuclear Excavations. Lawrence Radiation Lab., UCRL-7657, 1964. 46 pp.
6. Curry, R. L. Investigation of the Feasibility of Manufacturing Aggregate by Nuclear Methods. U. S. Army Engineer Waterways Exp. Sta., Misc. Paper No. 6-643, 1964. 19 pp.
7. Fisher, P. R. Large Diameter Drilling for Emplacing Nuclear Explosives. In Engineering with Nuclear Explosives, pp. 239-268. Proc. 3rd Plowshare Symposium, U. S. AEC, Div. of Tech. Info., TID-7695, 1964. pp. 239-268.
8. Frandsen, A. D. Pre-Schooner Postshot Exploration. U. S. Army Engineer Nuclear Cratering Group, Memo. 64-779, 1964.
9. Frank, W. J. The Characteristics of Nuclear Explosives. Lawrence Radiation Lab., UCRL-7870, 1964. 5 pp.
10. Hansen, S. M., and Lombard, D. B. Completely Contained Nuclear Explosives for Mining by Caving. In Engineering with Nuclear Explosives, pp. 371-384. Proc. 3rd Plowshare Symposium, U. S. AEC, Div. of Tech. Info., TID-7695, 1964.
11. Hansen, S. M., et al. Recommended Explosion-Crater Nomenclature. Geophysics, Vol. 29, No. 5, pp. 772-773, 1964.
12. Higgins, G. H. Evaluation of the Ground Water Contamination Hazard from Underground Nuclear Explosions. Jour. Geophysical Res., Vol. 16, No. 10, pp. 1509-1519, 1959.

13. Johnson, G. W., and Violet, C. E. Phenomenology of Contained Nuclear Explosions. Lawrence Radiation Lab., UCRL-5124, Rev. 1, 1958. 27 pp.
14. Johnson, G. W., Higgins, G. H., and Violet, C. E. Underground Nuclear Detonations. Lawrence Radiation Lab., UCRL-5626, 1959. 44 pp.
15. Leisek, J. F. Post-Shot Geologic Investigations of the Danny Boy Nuclear Cratering Experiment in Basalt. Lawrence Radiation Lab., UCRL-7803, 1964. 29 pp.
16. Nordyke, M. D. On Cratering—A Brief History, Analysis and Theory of Cratering. Lawrence Radiation Lab., UCRL-6578, 1961. 72 pp.
17. Nordyke, M. D., Nuclear Excavation Technology. Lawrence Radiation Lab., UCRL-7658, 1964. 23 pp.
18. Nordyke, M. D., and Wray, W. R. Preliminary Summary Report, Project Danny Boy. Lawrence Radiation Lab., UCRL-6999, 1962. 39 pp.
19. Pokrovskii, G. I., Fedorov, I. S., and Dokuchaev, M. M. Theory and Practice of Dam Construction by Directed Explosions. Transl. Lawrence Radiation Lab., UCRL-Trans-1035(L), 1951. 154 pp.
20. Rabb, D. D. Block Caving, Nuclear Style. Mining Eng., Vol. 16, No. 3, pp. 48-52, 1964.
21. Shelton, A. V., Nordyke, M. D., and Goeckermann, R. H. The Neptune Event—A Nuclear Explosive Cratering Experiment. Lawrence Radiation Lab., UCRL-5766, 1960. 32 pp.
22. Skrove, J. W., and McArthur, R. D. Post-Shot Geologic Studies of the Excavations in Neptune Crater. Lawrence Radiation Lab., UCRL-6812-T, 1962. 28 pp.
23. Stead, F. W. Distribution in Groundwater of Radionuclides from Underground Nuclear Explosions. In Engineering with Nuclear Explosives. pp. 127-138. Proc. 3rd Plowshare Symposium, U. S. AEC, Div. of Tech. Info., TID-7695, 1964.
24. Thompson, T. L., and Misz, J. B. Geologic Studies of Underground Nuclear Explosions Rainier and Neptune—Final Report. Lawrence Radiation Lab., UCRL-5757, 1959. 58 pp.
25. Todd, D. K. Economics of Ground Water Recharge by Nuclear and Conventional Means. Lawrence Radiation Lab., UCRL-7850, 1964. 135 pp.
26. Warner, S. E., and Violet, C. E. Properties of the Environment of Underground Nuclear Detonations at the Nevada Test Site, Rainier Event. Lawrence Radiation Lab., UCRL-5542, 1959. 21 pp.
27. Zodtner, H. H. Operations and Safety Problems Associated with a Nuclear Excavation Project. Lawrence Radiation Lab., UCRL-7656, 1964. 18 pp.
28. Crushed Stone. Rock Mining and Processing, Vol. 68, No. 1, pp. 60-61, Jan. 1965.

Appendix A

NUCLEAR CRATERING EXPERIMENTS IN ROCK

(Listed in Order of Increasing Scaled Depth of Burst)

Cratering Depth (Scaled Depth of Burst Less Than 200)

Buckboard No. 11—Explosive type, TNT; yield, 20 tons; scaled depth of burst, 81; depth of burial, 25.5 ft; rock type, basalt; apparent crater radius, 44.7 ft; apparent crater depth, 24.9 ft; firing date, Sept. 14, 1960; location, Buckboard Mesa, NTS.

Pre-Schooner Delta—Explosive type, nitromethane; yield, 20 tons; scaled depth of burst, 132.5; depth of burial, 41.8 ft; rock type, basalt; apparent crater radius, 46.1 ft; apparent crater depth, 25.6 ft; firing date, Feb. 27, 1964; location, Buckboard Mesa, NTS.

Buckboard No. 12—Explosive type, TNT; yield, 20 tons; scaled depth of burst, 135; depth of burial, 42.7 ft; rock type, basalt; apparent crater radius, 57.0 ft; apparent crater depth, 34.7 ft; firing date, Sept. 27, 1960; location, Buckboard Mesa, NTS.

Danny Boy—Explosive type, nuclear; yield, 0.42 ± 0.08 kt (1 kt equivalent to the explosive release of 10^{12} calories of energy and approximately equal to the energy released by the detonation of 1,000 tons of TNT); scaled depth of burst, 142; depth of burial, 110 ft; rock type, basalt; apparent crater radius, 107 ft; apparent crater depth, 62 ft; firing date, March 5, 1962; location, Buckboard Mesa, NTS.

Pre-Schooner Bravo—Explosive type, nitromethane; yield, 20 tons; scaled depth of burst, 159; depth of burial, 50.2 ft; rock type, basalt; apparent crater radius, 49.0 ft; apparent crater depth, 25.5 ft; firing date, Feb. 13, 1964; location, Buckboard Mesa, NTS.

Pre-Schooner Alfa—Explosive type, nitromethane; yield, 20 tons; scaled depth of burst, 184; depth of burial, 58.0 ft; rock type, basalt; apparent crater radius, 50.3 ft; apparent crater depth, 22.9 ft; firing date, Feb. 6, 1964; location, Buckboard Mesa, NTS.

Sulky—Explosive type, nuclear; yield, 87 ± 4 tons; scaled depth of burst, 184; depth of burial, 90 ft; rock type, basalt; average rubble mound radius, 79 ft; average rubble mound height, 21 ft; firing date, Dec. 18, 1964; location, Buckboard Mesa, NTS.

Buckboard No. 13—Explosive type, TNT; yield, 20 tons; scaled depth of burst, 186; depth of burial, 58.8 ft; rock type, basalt; apparent crater radius, 36.8 ft; apparent crater depth, 16.2 ft; firing date, Aug. 24, 1960; location, Buckboard Mesa, NTS.

Neptune—Explosive type, nuclear; yield, 115 ± 15 tons; scaled depth of burst, 189 (normal distance to nearest surface); vertical depth of burial, 109.5 ft; shortest distance to surface, 98.5 ft; rock type, welded tuff; apparent crater radius, 100 ft; apparent crater depth, 35 ft; firing date, Oct. 14, 1958; location, Rainier Mesa, NTS.

Intermediate Depth (Scaled Depth of Burst Between 200 and Containment)

Pre-Schooner Charlie—Explosive type, nitromethane; yield, 20 tons; scaled depth of burst, 210; depth of burial, 66.1 ft; rock type, basalt; rubble mound radius, 130 ft; average rubble mound height, 15.9 ft; firing date, Feb. 25, 1964; location, Buckboard Mesa, NTS.

Blanca—Explosion type, nuclear; yield, 19.0 ± 1.5 kt; scaled depth of burst, 312; vertical depth of burial, 988 ft; shortest distance to surface, 835 ft; rock type, welded tuff; depth of collapse crater at surface, 25 ft; approximate tonnage of rock broken, 22 million tons; firing date, Oct. 30, 1958; location, Rainier Mesa, NTS.

Containment[1] Depth (Buffer of Rock 300 Ft Thick Overlying Collapse Chimney)

Shoal—Explosion type, nuclear; yield, 12.5 kt; scaled depth of burst (for containment explosions measured in units of feet/$W^{1/3}$ rather than feet/$W^{1/3.4}$ used for cratering and intermediate depth explosions), 520; depth of burial, 1,205 ft; rock type, granite; cavity radius, 84 ft; chimney height, 356 ft; approximate tonnage of rock broken, 750,000 tons; location, Churchill County, Nevada.

Hardhat—Explosion type, nuclear; yield, 5.0 kt; scaled depth of burst, 550; depth of burial, 939 ft; rock type, granodiorite; cavity radius, 63 ft; chimney height, 281 ft; approximate tonnage of rock broken, 250,000 tons; location, Climax Stock, NTS.

Rainier—Explosion type, nuclear; yield, 1.7 kt; scaled depth of burst, 663; depth of burial, 899 ft; rock type, welded tuff; cavity radius, 65 ft; chimney height, 386 ft; approximate tonnage of rock broken, 500,000 tons; location, Rainier Mesa, NTS.

[1] Containment is used here to mean that gross explosion effects, such as surface subsidence, the ejection of rock fragments, and rubble mound formation, are prevented from developing at the surface by rock overlying the explosion. Contained, therefore, does not necessarily mean that radioactive by-products from the explosion do not reach the surface by seepage through fractures or other means. In other words, the explosion but not necessarily all of the radioactivity, is contained. Containment can usually be achieved by a buffer zone from 300 to 500 ft thick, depending on rock characteristics, overlying the gravity collapse rubble chimney.

Appendix B

SUMMARY OF HARD ROCK CRATERING DATA

Event[a]	Yield[b] (tons)	Explosive[c]	Dob (ft)	Dob′[d] $\left(\frac{ft}{kt^{1/3.4}}\right)$	R_a (ft)	R_a'[d] $\left(\frac{ft}{kt^{1/3.4}}\right)$	D_a (ft)	D_a'[d] $\left(\frac{ft}{kt^{1/3.4}}\right)$	Scaled Volumes[e] (10^4 cu yd/$kt^{0.88}$)				
									V_{br}'[f]	V_t'[g]	V_a'	V_{fb}'[i]	V_e'[j]
Buckboard No. 11	20	TNT	25.5	81	44.7	142	24.9	79	7.83	8.9	6.2	2.7	8.25
Pre-Schooner Delta	20	CH_3NO_2	41.8	132	46.1	146	25.6	81	14.0	15.7	7.46	8.24	14.86
Buckboard No. 12	20	TNT	42.7	135	57.0	180	34.7	110	21.33	22.4	15.5	6.9	23.0
Danny Boy	420	Nuclear	110	142	107	139	62	80	14.5	16.1	7.28	8.82	12.18
Pre-Schooner Bravo	20	CH_3NO_2	50.2	159	49.0	155	25.5	81	19.43	20.5	8.75	11.75	15.45
Pre-Schooner Alfa	20	CH_3NO_2	58.0	183	50.3	159	22.9	73	23.53	24.6	8.74	15.86	17.14
Buckboard No. 13	20	TNT	58.8	186	36.8	117	16.2	51	14.03	15.1	2.66	12.44	7.16
Neptune	115	Nuclear	98.5	189	100	189	35.0	66	29	30	14.7	15.3	22.8[k]
Pre-Schooner Charlie	20	CH_3NO_2	66.1	210	R-57[l]	180	—	—	36.9	38.0	—	51.8	—

[a]With exception of Neptune, all events tabulated were fired in basalt on Buckboard Mesa at AEC Nevada Test Site.

[b]Yields of high explosives shown are actual charge weights with 1 ton = 2,000 lb of explosive; Nuclear yields are defined as 1 ton = 10^9 calories.

[c]Twenty-ton TNT charges are formed from 36-lb blocks of cast TNT (density of 1.53 gm/cu cm) stacked to approximate spherical charge. Nitromethane (CH_3NO_2) is liquid used primarily as solvent; under conditions of confinement, it can be made to detonate with properties similar to TNT. The 20-ton charges were contained in leak-tight spherical cavities.

[d]Dob′, R_a', D_a' are scaled depth of burst, apparent crater radius, and apparent crater depth, respectively; yield in kilotons to $^1/_{3.4}$ power is scaling factor; scaled dimensions shown would be real dimensions for yield of 1 kt.

[e]Scaling of volumes as 0.88 power of yield for cratering shots is natural consequence of cubing dimensions which are scaled to $^1/_{3.4}$ power of explosive yield; i.e., $\left(kt^{1/3.4}\right)^3 = kt^{0.88}$. Volumes for completely contained shots are directly proportional to yield since chimney height is linear function of cavity radius which scales as yield to $^1/_3$ power.

[f]V_{br}' is total scaled volume of in-situ rock broken and available for aggregate. It is calculated as volume of true crater, V_t', minus volume of initial spherical cavity formed on detonation. Computed V_{br}' is conservative since much broken rock in rupture zone outside true crater surface which is also available for aggregate is not included. An in-situ density of 2.6 gm/cu cm was used to determine tonnage from V_{br} column for Figure 2.

[g]V_t' is scaled volume of true crater. It is assumed that apparent crater radius and true crater radius are equal. V_t' is calculated as volume of a right circular cone frustum plus lower cavity hemisphere. R_c', lower cavity radius, R_a', and Dob′ are frustum parameters.

[h]V_a' is scaled apparent crater volume, determined from preshot and postshot topographic maps of crater area for actual crater. Actual volumes are scaled to 1 kt by dividing by W in $kilotons^{0.88}$.

[i]V_{fb}' is scaled volume of fallback material or material which was placed in trajectory but landed inside crater; it is computed as $V_t' - V_a'$.

[j]V_e' is scaled volume of ejecta or material placed in trajectory which lands outside the crater. This is most easily available source of aggregate. An accurate determination of V_e is difficult. Apparent lip volumes from topographic maps must be used with supporting data from trenches cut through lip to determine volume of true lip. The simple approach used here is to assume a swell factor for V_{br} and to conserve this mass, or $V_e = (S)\,V_{br} - V_{fb}$. A swell factor of 1.65 is used for Pre-Schooner Delta and 1.45 for Danny Boy. In the absence of field data, S = 1.40 is used for all other craters.

[l]True crater radius, R_t has been estimated based on cross-section shown in Figure 4.

[k]V_e' shown for Neptune includes only material in slide area since approach used in note j is not applicable.

Progress in Nuclear Excavation Technology

MILO D. NORDYKE, University of California, Lawrence Radiation Laboratory, Livermore, California; and
LOUIS J. CIRCEO, U. S. Army Corps of Engineers

Several experiments conducted during the past year in the Plowshare Program and other developments related to nuclear cratering are described. Newly developed cratering curves in alluvium and basalt rock are presented, based on several high-explosive cratering programs. Progress in the development of a theoretical model of cratering is summarized. Also described is a recent investigation into the phenomenology of subsidence craters produced by very deeply buried detonations in alluvium. High-explosive row charge detonations to produce channels are presented. Results from the Dugout experiment, the first row charge cratering detonation in rock, indicated that many of the concepts developed for row charges in alluvium are also valid in a hard rock medium.

Two investigations into the survival of craters under the action of natural and dynamic forces are described, and economics of nuclear excavation are presented using newly released AEC charges for nuclear explosives. Advancement in the development of low-fission thermonuclear explosives is expected to reduce radioactivity levels considerably below 1962 Sedan levels.

•THE PLOWSHARE Program was established in 1957 to investigate possible industrial applications of nuclear explosives. Currently under investigation are applications relating to excavation, mining, and isotope production. Large-scale excavation is perhaps the most promising use of nuclear explosives. The great energy released by a buried nuclear explosion shatters and imparts a sufficient velocity to the medium above the explosion not only to break up the medium, but also to eject it and produce a crater. A row of explosions spaced about one crater radius apart and detonated simultaneously will produce a ditch about the depth and width of a single crater. Such effects indicate a potential capability of nuclear explosives for excavating large quantities of material for the construction of harbors, canals, and highway and railway cuts. Deeper burial in a hard rock medium would produce large quantities of broken rock which could be used as aggregate.

Over the past 13 years a considerable body of data on explosive cratering has been developed for application to nuclear excavation projects (1). These data were obtained from ten cratering programs using chemical high explosives and seven nuclear cratering detonations. The types of media studied have ranged from marine muck to hard dry basalt, although most effort has been devoted to craters in desert alluvium and basalt at the Nevada Test Site. Considerable effort has also been devoted to the study, with chemical explosives, of the use of linear explosives and rows of point charges. Basic nuclear excavation technology has previously been discussed (2). This paper summarizes information acquired during the past year which has contributed toward nuclear excavation technology and industrial applications.

DEVELOPMENT OF NUCLEAR EXCAVATION TECHNOLOGY

Cratering in Alluvium

Table 1 summarizes most of the pertinent nuclear cratering data obtained since 1951. Not shown is a large amount of data obtained from explosions at much larger depths

Paper sponsored by Special Committee on Nuclear Principles and Applications.

TABLE 1

SUMMARY OF NUCLEAR CRATERING DATA FROM NEVADA TEST SITE

Shot Name	Medium	Yield (kt)	Dimensions of Apparent Crater				
			Depth of Burst (ft)	Radius (ft)	Depth (ft)	Volume (cu yd)	Lip Height (ft)
Jangle S	Alluvium	1.2 ± 0.1	-3.5[a]	45	21	1.65×10^3	—
Johnnie Boy	Alluvium	0.5 ± 0.2	1.75	61	30	5.3×10^3	10
Jangle U	Alluvium	0.2 ± 0.1	17	130	53	3.7×10^4	8
Teapot ESS	Alluvium	1.2 ± 0.1	67	146	90	9.6×10^4	20
Sedan	Alluvium	100 ± 15	635	604	320	6.6×10^6	15-100
Danny Boy	Basalt	0.42 ± 0.08	110	107	62	3.6×10^4	15-30
Neptune[b]	Tuff	0.115 ± 0.015	100	100	35	2.2×10^4	—

[a]Detonated 3.5 ft above surface. [b]Detonated 100 ft beneath a 30-deg slope.

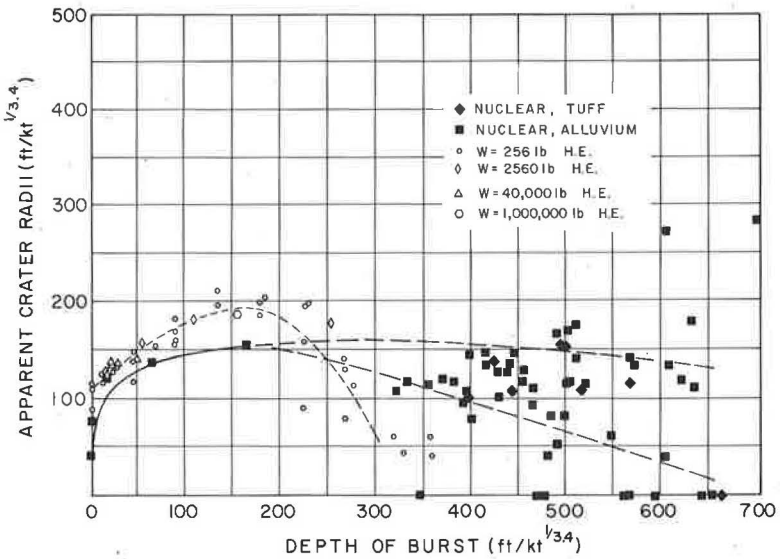

Figure 1. Plot of chemical high explosive (H.E.) and nuclear explosive apparent crater radius data vs depth of burst; NTS desert alluvium, $W^{1/3.4}$ scaling.

of burst. Nuclear and chemical explosive data points for desert alluvium have been plotted in Figures 1 and 2. The dashed curves are the last-square fits of the 256-lb chemical explosive data. Nuclear data are shown by the solid curves. The difference between the curves for the chemical explosive and those for nuclear explosive data is attributed to the variation of explosion phenomena between nuclear and chemical explosives (3).

Much data have also been obtained from the nuclear weapons tests conducted at the Nevada Test Site over the past several years. When a large nuclear explosion is detonated at a depth of burial much deeper than optimum, a large underground cavity is formed which ultimately collapses, resulting in a large subsidence crater at the surface of the ground. Figure 3 shows a schematic cross-section of such a crater as reconstructed from postshot drill-hole information. Figure 4 is a photograph of a typical subsidence crater a few seconds after it has collapsed. The data points for a large number of these subsidence craters whose scaled depths of burial vary from 300 to 700 $ft/kt^{1/3.4}$ have been plotted in Figures 1 and 2. In some cases, the detonation point was located in weakly cemented tuff; in others, it was located in alluvium. In all cases, the

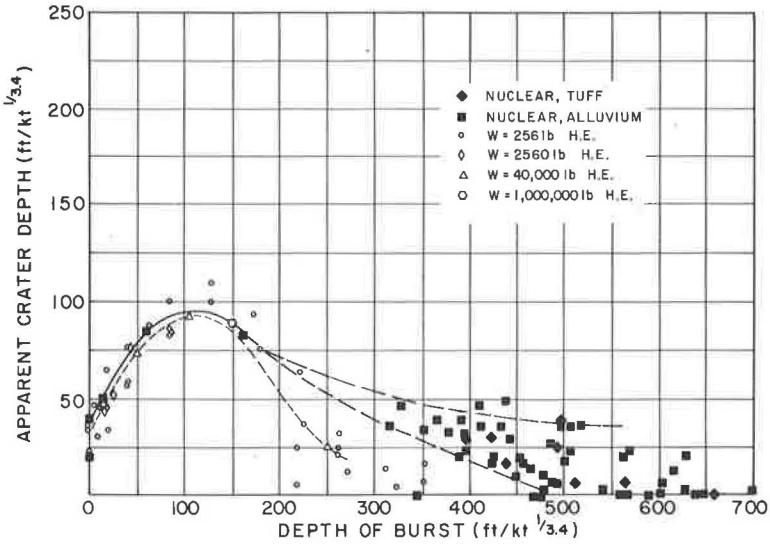

Figure 2. Plot of chemical high explosive (H.E.) and nuclear explosive apparent crater depth data vs depth of burst; NTS desert alluvium, $W^{1/3.4}$ scaling.

major portion of the collapse chimney region was in alluvium. The nature of the medium surrounding the detonation point is indicated.

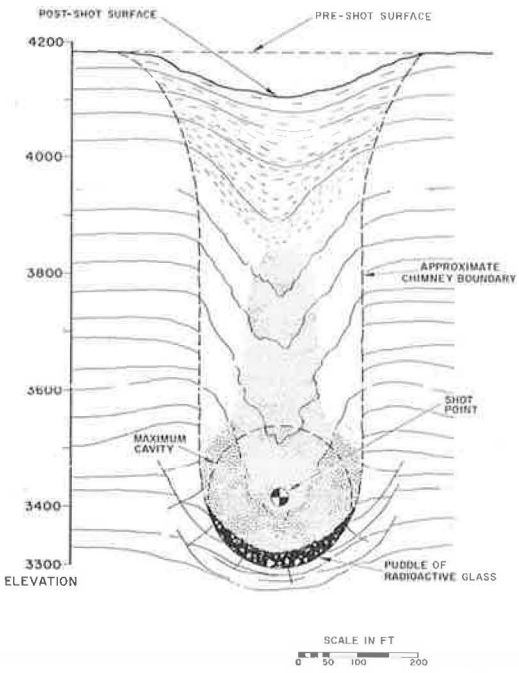

Figure 3. Schematic cross-section of typical subsidence crater in alluvium.

These subsidence cratering data for large-yield explosions have had a significant effect on our predictions of the size craters expected at large depths of burial in desert alluvium. It should be noted that subsidence craters are only expected in a medium such as desert alluvium where no bulking during collapse is observed. In a rock-type medium where bulking does occur, the volume of the underground cavity would not be transmitted to the surface as it is in alluvium, but would be distributed throughout the chimney region in the form of voids between the broken rock. With deep burial, the collapse region would, in fact, not even reach the surface of the ground.

Cratering in Basalt

To obtain cratering data for hard rock that would be useful to the Plowshare Program, Project Buckboard was undertaken in the summer of 1960. This program consisted of ten 1,000-lb and three 40,000-lb detonations in basalt (4). The site was a basalt-topped mesa in the Forty-Mile Canyon area on the west side

Figure 4. Aerial view of typical subsidence crater taken several seconds after collapse.

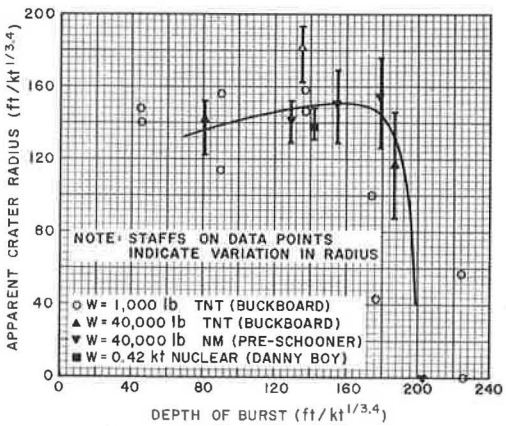

Figure 5. Plot of chemical high explosive (H.E.) and nuclear explosive apparent crater radius data vs depth of burst; basalt, $W^{1/3.4}$ scaling.

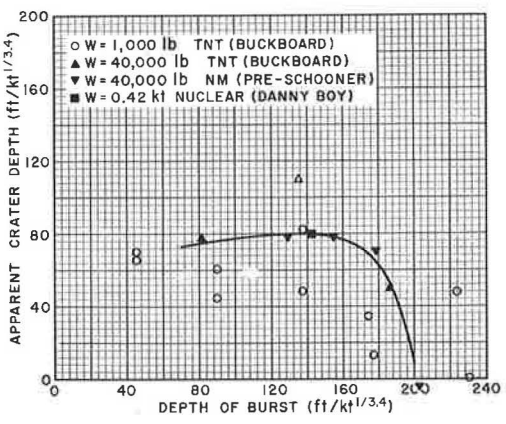

Figure 6. Plot of chemical high explosive (H.E.) and nuclear explosive apparent crater depth data vs depth of burst; basalt, $W^{1/3.4}$ scaling.

of the Nevada Test Site. These data are plotted in Figures 5 and 6. Visual observation of the craters led to the conclusion that 1,000-lb charges in a hard rock such as basalt do not result in meaningful apparent crater data. The apparent craters for the 40,000-lb charges, however, appeared to be much more relevant. It should be mentioned that the crater resulting from the intermediate shot at 136 ft/kt$^{1/3.4}$ was half in cinders and half in solid basalt. The effect of this on crater dimensions was somewhat difficult to estimate, but the unusually large dimensions of this crater relative to the other craters made this data point appear somewhat anomalous.

In an effort to obtain more and better data in basalt, a cratering program was undertaken in the spring of 1964 by the U.S. Army Engineer Nuclear Cratering Group (5). This program, called Pre-Schooner, was conducted at the same site as the Buckboard series and consisted of four 40,000-lb shots using the liquid chemical explosive, nitromethane. These data are also plotted on Figures 5 and 6.

Shown in Figures 5 and 6 are curves fit to these data. The 1,000-lb crater data and the data point for the anomalous Buckboard crater at 136 ft/kt$^{1/3.4}$ were given essentially no weight. Comparison of the 1,000-lb and the 40,000-lb crater data does not allow derivation of an empirical scaling exponent for basalt, but it does indicate that a scaling such as $W^{1/3.4}$ is adequate.

Row Charge Data

Alluvium.—Since Plowshare is interested in the utilization of craters for purposes such as canals and railroad and highway cuts, we are interested in the effects not only of point charges but also of rows of charges detonated simultaneously.

Figure 7. Vertical aerial view of Pre-Buggy crater in Area 5, NTS.

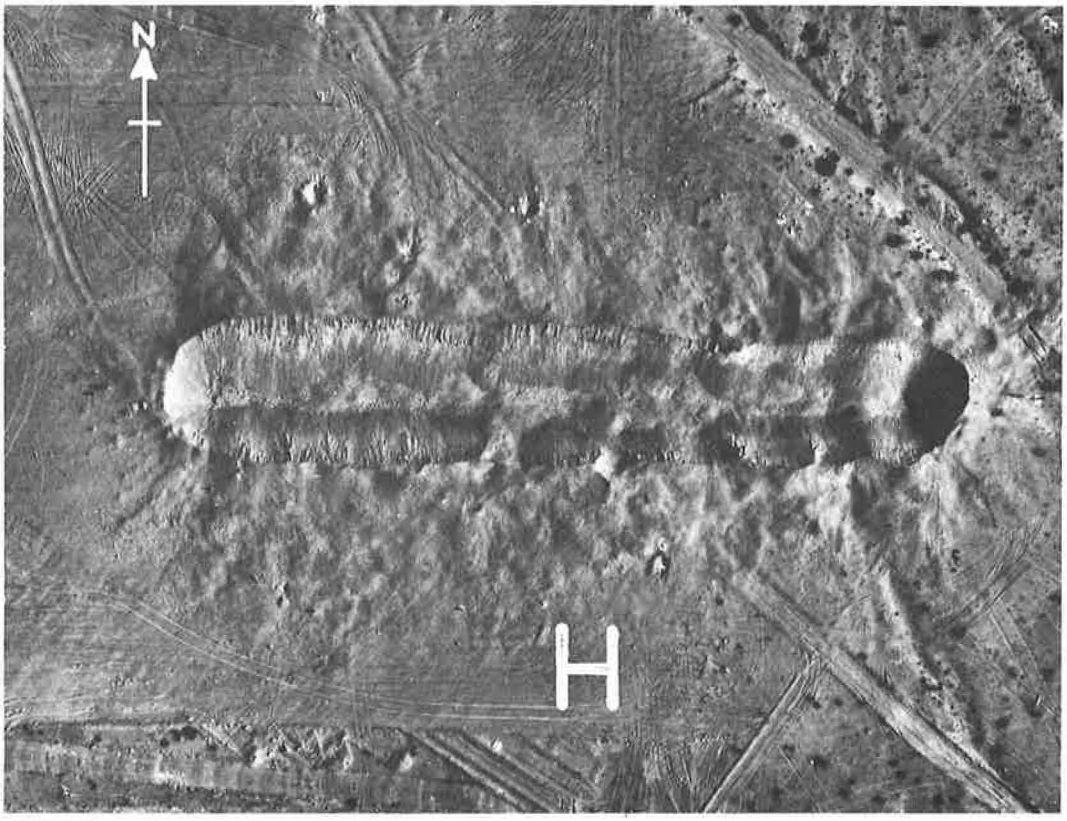

Figure 8. Vertical aerial view of Pre-Buggy crater H, showing effect of change of spacing from 1 radius spacing on the left to $1\frac{1}{2}$ spacing on the right.

In 1963, the U. S. Army Engineer Nuclear Cratering Group conducted the Pre-Buggy Program (6), consisting of a number of cratering shots utilizing 1,000-lb charges of nitromethane. Each detonation consisted of five charges in a row detonated simultaneously. In an extension of this program in July 1963, conducted by the Lawrence Radiation Laboratory and termed Pre-Buggy II (7), these cratering data were extended to two unique geometries: (a) two craters connected end-on in an attempt to explore the problem of connecting two craters, and (b) 13 charges using the same depth of burst but three different spacings. The Pre-Buggy area is shown in Figure 7. The two connecting craters are shown in the Pre-Buggy II area and are labeled C′ and C. The 13 charges with three different spacings are labeled row H.

The purpose of these row cratering experiments was to determine: (a) the effect on crater dimensions of variation in the spacing between charges, (b) the effect of spacing on the irregularity or cusping in the crater, and (c) the shape of the lip relative to the lip obtained with point charges, on both the sides and the ends of the crater. The conclusions can be summarized as follows:

1. Use of a spacing equal to approximately a single crater radius results in a smooth-sided crater with apparent dimensions about 10 to 20 percent larger than expected on the basis of single charge data;
2. Use of a spacing of about 1.25 times a single crater radius results in a ditch with dimensions approximately equal to those expected from single charges; and
3. Use of a spacing of 1.5 times a single crater radius results in a crater which is somewhat smaller than a single crater radius and quite irregular in cross-section.

These three spacings were used for row H, and the effect of the various spacings can be seen in Figure 8, an aerial view of row H, Pre-Buggy II.

The other significant conclusion from these cratering programs is that when four, five, or more charges in a row are fired simultaneously under conditions that result in a uniform ditch, the lips on the sides of the crater are approximately 50 to 100 percent higher than would be expected from single crater lips, whereas the lip on the end of the crater is virtually nonexistent in alluvium. This effect, of course, is extremely

Figure 9. Dugout crater.

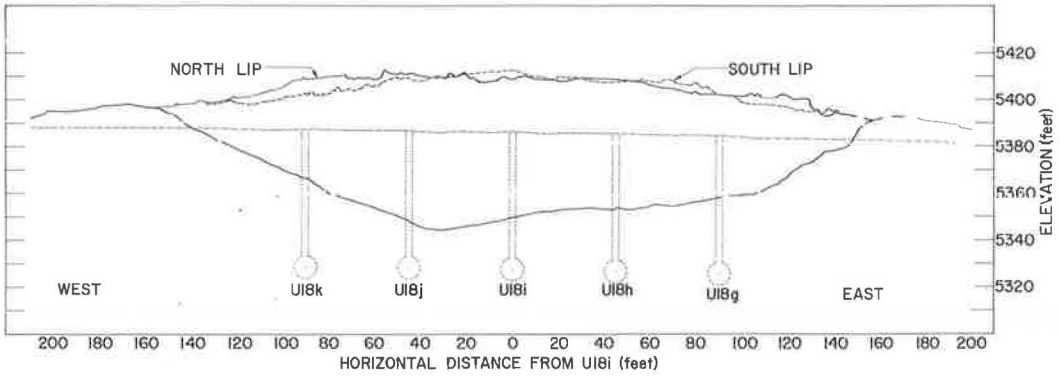

Figure 10. Cross-section and plan view of crater resulting from Dugout detonation.

significant when one is discussing the concept of making a long channel where it is necessary to connect a number of ditches.

Basalt.—Since most nuclear excavation applications will be in hard rock, it is regarded as extremely important to extend row charge data to that medium. In June 1964, the Dugout experiment, the first row cratering experiment in hard rock, was conducted on Buckboard Mesa at the Nevada Test Site (8). This project consisted of five spheres, each containing 40,000 lb of nitromethane.

The center of each sphere was about 59 ft below the ground surface, corresponding to a scaled depth of burst of about 185 $W^{1/3.4}$. The charges were spaced 45 ft apart, which corresponded to a spacing of slightly less than one crater radius. Five additional emplacement holes were drilled on line with the experiment to determine the damage incurred by emplacement holes adjacent to cratering explosions.

The crater resulting from the detonation is shown in Figure 9, and a plan and cross-section view is shown in Figure 10. The average width of the center 60 percent of the crater is 136 ft. The average depth of the crater is 35 ft, and the length is 287 ft. The average lip height above the original ground surface is about 24 ft along the sides of the crater and 12 ft on the ends. The apparent crater has a volume of about 21,000 cu yd.

The Dugout experiment produced several interesting conclusions regarding row cratering in a rock medium. Assuming that the 45-ft spacing is equivalent to the spacing of a single crater in this location, an enhancement of greater than 30 percent is seen in the crater dimensions of width and depth. This is similar to the enhancement observed in the Pre-Buggy series. The lip height along the sides was about 65 percent of the crater depth, also similar to Pre-Buggy. However, the lips on the ends were somewhat greater than those observed in alluvium. Perhaps the most significant results are that the simultaneous detonation of a row of explosives will produce a linear channel with no cusps and that many of the concepts developed for row charges in alluvium appear to also be valid in a hard rock medium.

Engineering Developments

Over the past several years, several nuclear detonations have taken place at the Pacific Proving Grounds at Eniwetok and Bikini Atolls. Many of these shots were surface and near-surface bursts which resulted in craters, some of considerable size. Figure 11 shows three of the Pacific craters. The two large craters, Mike and Koa, were produced by high-yield detonations, and the small crater, Seminole, was a low-yield shot. The Mike crater is over 1 mi in diameter.

In April 1964, a study was conducted at Eniwetok Atoll to investigate the long-term effects of wave action and weathering on craters (9). This study has indicated that no major changes have occurred in the craters, except for considerable silting up of the large craters shown in Figure 11. Minor slope failures have occurred and wave action has eroded the above-water lips of some craters. However, the craters have significantly altered the geomorphic balance of wave action, erosion, and deposition in the area. Burial at optimum depth will result in higher lips, steeper slopes, and more protection from external weathering conditions.

In another study, an investigation is being conducted into the ability of cratered slopes to survive ground shock from adjacent detonations. The 100-kt Sedan crater was instrumented and photographed in conjunction with a nearby underground detonation to observe the slope reaction to the seismic shock. Preliminary results indicate that portions of the crater received ground shocks in excess of 1.0 g. Only minor slope failures occurred, all in sections previously considered unstable, indicating that cratered splopes can withstand considerable ground shock from adjacent detonations. This becomes important when joining or extending nuclear channels. Only an insignificant amount of the rockfall resulting from these minor slope failures rolled to the bottom of the crater where a roadway would ordinarily be located in a nuclear-excavated highway cut.

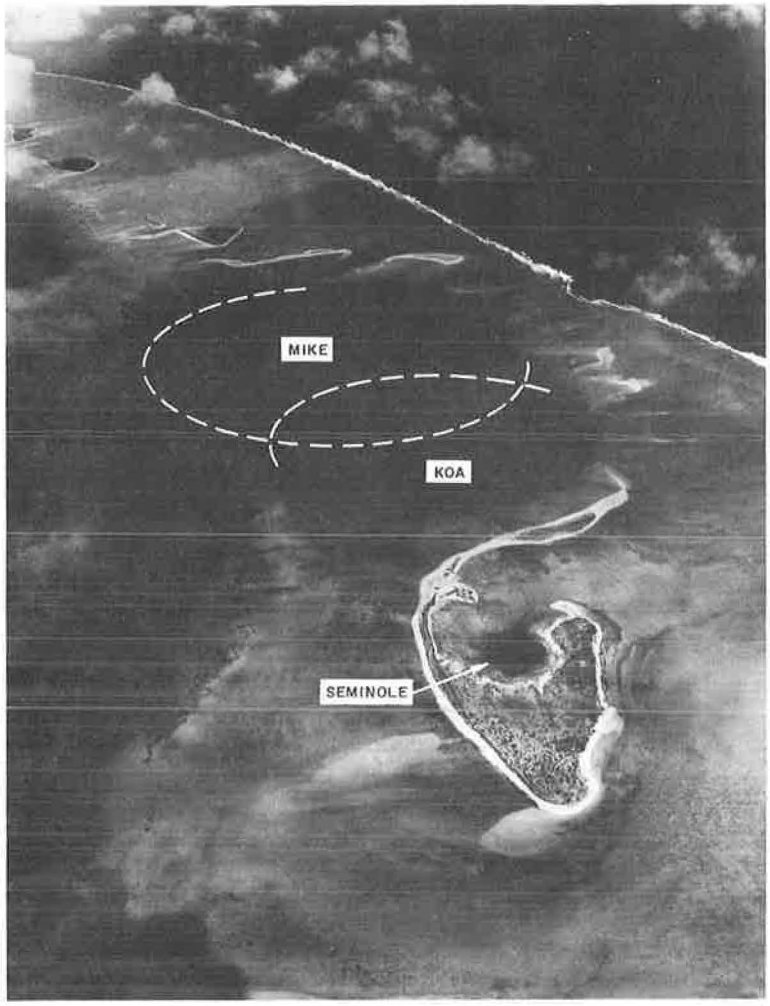

Figure 11. Craters produced by near-surface detonations at Pacific Proving Grounds, Eniwetok Atoll.

Theoretical Calculations of Cratering Mechanics

In an effort to develop a more fundamental understanding of the cratering process and the interaction of the various parameters encountered in nature, considerable effort has been devoted to the development of a theoretical calculation of the cratering process. Present work is based on a two-phase model (3) which considers first the hydrodynamic growth of a spherical cavity resulting from the explosion. When the rarefaction would be expected to return to the cavity from the earth's surface, this model is no longer valid. The second phase of the cavity growth is the so-called gas-acceleration phase resulting from the adiabatic expansion of the cavity in the upper hemisphere with a resultant long-term acceleration of the overlying medium.

The first phase is calculated on a one-dimensional hydrodynamic plastic-elastic computer code called SOC (10). The output from this code establishes the initial conditions of the cavity size, cavity pressure, and particle velocity of the medium between the cavity and the ground surface that are required for the second phase of the calculation.

For this second phase, the overburden material is assumed to be a homogeneous, incompressible, viscous fluid. The upper cavity surface is subdivided into elemental surface areas, and mass zones are defined which subtend these areas. By applying Newton's Second Law with simple empirically calibrated frictional force to each mass element and assuming that the cavity gas behaves adiabatically, the cavity evolution, mound development, and the formation of the lip through upthrust are numerically simulated.

These calculational models have been applied (11) to the 0.5-kt chemical cratering explosion, Scooter, and have reproduced observed ground motions extremely well. In addition, the models have been used to calculate a 0.5-kt chemical explosive source at a variety of depths of burst. Assuming a reasonable angle of repose for alluvium of 45 deg, crater radii for scaled depths of burst from about 30 to 200 $ft/kt^{1/3.4}$ have been predicted which compare very favorably with observed crater radii for chemical explosives in alluvium. Further, the apparent crater depths for shallow depth of burst craters have been reasonably well calculated.

RELATED DEVELOPMENTS

Nuclear Device Charges

The AEC has encouraged industry and other groups to participate in the Plowshare Program by analyzing the possible uses of nuclear explosives in their specific fields.

TABLE 2

ESTIMATED UNIT COSTS OF EXCAVATION IN HARD ROCK

Yield (kt)	Projected Charge ($)	Depth of Burial (ft)	Cost of Emplacement Hole[a] ($)	Operations and Safety Cost[b] ($)	Total Cost ($)	Apparent Crater Dimensions			Unit Cost ($/cu yd)
						Diameter (ft)	Depth (ft)	Volume (cu yd)	
10	350,000	280	84,000	200,000	634,000	540	155	660,000	0.96
100	460,000	550	165,000	300,000	925,000	1,070	310	5,160,000	0.18
2,000	600,000	1,330	400,000	500,000	1,500,000	2,580	750	72,220,000	0.02

[a]Assuming drilling costs of $300/ft.
[b]Varies greatly from one site to another; for this comparison a typical cost averaged over a number of charges in a row has been assumed.

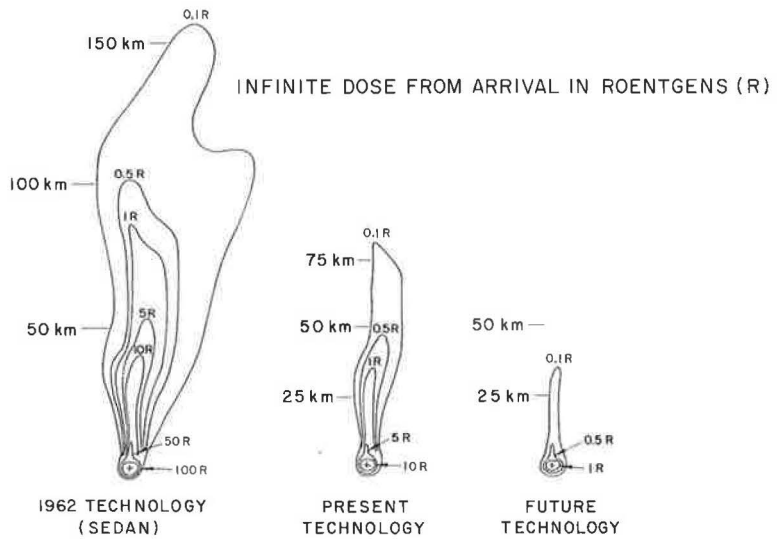

Figure 12. Estimated technological advances to be made in fallout deposition of radioactive debris from 100-kt nuclear cratering detonation.

To allow such investigations, the Commission in 1958 released, within the limits permitted by national defense and security, a schedule of cost estimates for nuclear explosives and related services, including safety studies.

Since that time, improvements have been made both in the design of nuclear explosives and in their emplacement, as well as in the technology of the explosion and its effects. One of the most significant technological advances has been in the development of thermonuclear explosives with very low fission yields.

Consequently, in 1964 the AEC revised its estimates and now projects a charge of $350,000 for a nuclear explosive with 10-kt yield and $600,000 for a nuclear explosive with 2-megaton yield (12). Interpolations may be made for other yields based on a line drawn between these two charges (13, Fig. 13). These charges cover nuclear materials, fabrication and assembly, and arming and firing services. Significant related services which are not covered by these projected charges are safety studies, site preparation including construction of holes, transportation and emplacement of the devices, and support. Costs of safety studies, which were included in the 1958 charges, have not been included in the new charges since they can be accurately estimated only for each individual situation.

It is expected that these projected charges are sufficiently representative of the future situation to warrant their use in feasibility studies. Although the projected charges might be used as a basis for discussion of costs to be assumed by the AEC in such projects, it should be recognized that the costs to be assumed by the AEC as finally negotiated might be significantly different from the projected charges.

Using these charges and assuming related excavation costs, it is significant to note the estimated costs of nuclear excavation. As shown in Table 2, excavation in the 10-kt range produces unit excavation costs which are competitive with conventional excavation costs. However, using larger yields, the unit cost is reduced rapidly to a few cents per cubic yard in the megaton range. This emphasizes the great economic benefits to be derived from nuclear explosive techniques for large-scale excavation.

Radioactivity

As mentioned previously, recent technological advances have developed thermonuclear explosives with very low fission yields. In addition to economy in device charges, reduced fission yields greatly decrease the amount of radioactivity produced. This will significantly increase the radiological safety of nuclear excavation.

Figure 12 illustrates the advances being made in this area. The 1962 fallout pattern is based on the Sedan event. The infinite dose is that which downwind residents would receive, assuming continuous residency following a 100-kt nuclear detonation. The roentgen contour is approximately equal to the maximum lifetime dose allowed to the general population by the Federal Radiation Council.

As seen in Figure 12, the range to the 0.5-roentgen isodose line for a cratering explosion like Sedan would be about halved if present explosives had been used. Use of nuclear explosives and emplacement techniques which will be developed in the foreseeable future will effect an even more dramatic reduction of such a fallout pattern. These reductions mean that the amount of radioactive material in future fallout patterns from a 100-kt cratering explosion will be about a factor of 100 less than the amount in the 1962 Sedan fallout pattern.

SUMMARY

A large quantity of cratering data has been obtained over the past 13 years in a number of media. One medium in particular, NTS desert alluvium, has been exhaustively explored with both chemical explosive point charges, nuclear point charges, and chemical explosive row charges. One other medium, basalt, has been explored to a lesser extent with large-yield chemical explosive charges, and cratering curves have been determined. These two media, in general, are expected to bracket most types of media to be encountered in nature; therefore, the range of crater dimensions to be expected for many nuclear excavation projects will, in all probability, fall between these two types of media. The Dugout experiment, the first row charge cratering ex-

periment in hard rock, indicates that many of the concepts developed for row charges in alluvium are also valid in a hard rock medium.

Two investigations into the survival of craters under the action of natural and dynamic forces indicate that craters are not severely affected by wave and water action over long periods and that cratered slopes can survive large seismic forces without experiencing serious slope failures.

A theoretical model of explosive cratering is being developed, based on a hydroelastic-plastic model and a late-phase gas-acceleration model. Results to date are very encouraging and indicate an ability to duplicate both observed surface motions and empirical crater dimension curves for alluvium.

Nuclear excavation costs in hard rock are estimated to be competitive with conventional excavation in the 10-kt range, rapidly decreasing to a few cents per cubic yard in the megaton range. Advancement in the development of low-fission thermonuclear explosives in the near future is expected to reduce radioactivity levels 100-fold below 1962 Sedan levels.

In all, many significant developments have occurred during the past year which have brought nearer the fulfillment of such applications as Project Carryall and the construction of a new sea-level Isthmian Canal by nuclear methods.

REFERENCES

1. Nordyke, M. D. Cratering Experience with Chemical and Nuclear Explosives. Proc. 3rd Plowshare Symposium, Lawrence Radiation Lab., TID-7695, April 1964.
2. Nuclear Excavation, 1963. Highway Research Record No. 50, 1964. 53 pp.
3. Nordyke, M. D. On Cratering: A Brief History, Analysis and Theory of Cratering. Lawrence Radiation Lab., UCRL-6578, Aug. 1961.
4. Vortman, L. J., et al. Project Buckboard, Final Report. Sandia Corp., SC-4675(RR), Aug. 1962.
5. Spruill, J. L. Project Pre-Schooner, Crater Measurements. U. S. Army Engineer Nuclear Cratering Group, PNE-502, Nov. 1964.
6. Graves, E., et al. Project Pre-Buggy, Scope of Chemical Explosive Cratering Experiment. U. S. Army Engineer Nuclear Cratering Group, PNE-300, May 1963.
7. Spruill, J. L., and Videon, F. F. Project Pre-Buggy II, Apparent Crater Studies. U. S. Army Engineer Nuclear Cratering Group, PNE-315, Nov. 1964.
8. Nordyke, M. D., et al. Project Dugout, Technical Director's Summary Report. Lawrence Radiation Lab., PNE-600, Jan. 1965.
9. Circeo, L. J., and Nordyke, M. D. Personal communication.
10. Butkovich, T. R. Calculation of the Shock Wave from an Underground Nuclear Explosion in Granite. Proc. 3rd Plowshare Symposium, Lawrence Radiation Lab., TID-7695, April 1964.
11. Knox, J. B., and Terhune, R. W. Calculation of Explosion of Explosion-Produced Craters—High Explosive Sources. Lawrence Radiation Lab., UCRL-7738, Rev. I, Oct. 1964.
12. Frank, W. J. Characteristics of Nuclear Explosives. Proc. 3rd Plowshare Symposium, Lawrence Radiation Lab., TID-7695, April 1964.
13. Hansen, S. M., and Toman, J. Aggregate Production with Nuclear Explosives. Highway Research Record No. 107, 1966.